

# Symmetry of Magnetic Quantum Tunneling in the Single-Molecule Magnet $Mn_{12}$ -Acetate

E. del Barco and A. D. Kent

Department of Physics, New York University, 4 Washington Place, New York, NY 10003

S. Hill

Department of Physics, University of Florida, Gainesville, FL 32611-8440

J. M. North and N. S. Dalal

Department of Chemistry and National High Magnetic Field Laboratory, Florida State University, Tallahassee, FL 32306

E. M. Rumberger and D. N. Hendrickson

Department of Chemistry and Biochemistry, University of California San Diego - La Jolla, CA 92093-0358

N. Chakov and G. Christou

Department of Chemistry, University of Florida, Gainesville, FL 32611-7200

(Dated: May 23, 2019)

The symmetry of magnetic quantum tunneling (MQT) in the single molecule magnet  $Mn_{12}$ -acetate has been determined by sensitive low-temperature magnetic measurements in the pure quantum tunneling regime and high frequency EPR spectroscopy in the presence of large transverse magnetic fields. The combined data set definitively establishes the transverse anisotropy terms responsible for the low temperature quantum dynamics. MQT is due to a disorder induced locally varying quadratic transverse anisotropy associated with rhombic distortions in the molecular environment ( $2^{\text{nd}}$  order in the spin-operators). This is superimposed on a  $4^{\text{th}}$  order transverse magnetic anisotropy consistent with the global (average)  $S_4$  molecule site symmetry. The hard axes associated with these forms of the transverse anisotropy are not collinear, leading to a complex interplay between local and global symmetries, the consequences of which are analyzed in detail. The resulting model explains: (1) the observation of a twofold symmetry of MQT as a function of the angle of the transverse magnetic field when a subset of molecules in a single crystal are studied; (2) the non-monotonic dependence of the tunneling probability on the magnitude of the transverse magnetic field, which is ascribed to an interference (Berry phase) effect; and (3) the angular dependence of EPR absorption peaks, including the fine structure in the peaks, among many other phenomena. This work also establishes the magnitude of the  $2^{\text{nd}}$  and  $4^{\text{th}}$  order transverse anisotropy terms for  $Mn_{12}$ -acetate single crystals and the angle between the hard magnetic anisotropy axes of these terms. EPR and magnetic data are consistent with a  $2^{\text{nd}}$  order transverse anisotropy that is slightly larger for d- $Mn_{12}$ -acetate than that for h- $Mn_{12}$ -acetate. In addition, EPR as a function of the angle of the field with respect to the easy axis (close to the hard-medium plane) confirms that there are discrete tilts of the molecular magnetic easy axis from the global (average) easy axis of a crystal, seen previously in h- $Mn_{12}$ -acetate. These tilts are also associated with solvent disorder. The latter observation provides a very plausible explanation for the lack of MQT selection rules, which has been a puzzle for many years.

PACS numbers: 75.45.+j, 75.50.Tt, 75.60.Lr

## I. INTRODUCTION:

The origin of magnetic quantum tunneling (MQT) in single molecule magnets (SMMs) is important for fundamental reasons as well as proposed applications of SMMs, ranging from magnetic data storage to quantum computing [1, 2]. A macroscopic (millimeter-sized) SMM single crystal to a first approximation can be considered an ensemble of weakly interacting molecules with the same chemical composition and orientation. In this regard SMM single crystals are ideal materials in which to study the quantum properties of magnetic molecules, as the magnetic response is amplified by the huge number of molecules forming the crystal. The environment of the molecules in crystals is well defined and can be

characterized by techniques such as x-ray diffraction.

SMMs have a predominant uniaxial magnetic anisotropy that determines an easy magnetic axis for the spin. MQT is due to interactions that break this axial symmetry and lead to transitions between magnetic states with opposite projections of spin on the magnetic easy axis. While this is fundamental to their quantum dynamics, remarkably only recently have the nature of the transverse interactions that produce MQT been determined in the first and most studied SMM,  $Mn_{12}$ -acetate (henceforth  $Mn_{12}$ ) [3, 4, 5, 6, 7, 8, 9, 10, 11, 12, 13, 14, 15, 16, 17, 18, 19]. Small modulations in the local environment around the magnetic cores have been found to be important in MQT [16, 17, 18, 19]. In particular, it has also been shown

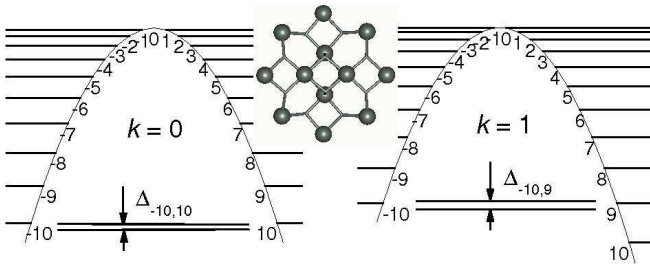


FIG. 1: Energy diagram of the  $2S + 1 = 21$  projections of the spin  $S = 10$  along the easy magnetic axis of the  $Mn_{12}$  molecule for resonances  $k = 0$  and  $k = 1$ . The tunnel splitting,  $\Delta_{m, m^0}$  ( $m + m^0 = k$ ), is illustrated in both cases. The inset shows the organization of the manganese ions looking down the  $S_4$  axis of the molecule ( $z$ -axis). Note the spins point up and down along this axis, perpendicular to the plane of the page.

that in  $Mn_{12}$  there are a variety of types of disorder that affect the magnetic properties of the molecules, including a distribution of solvent microenvironments,  $g$  and  $D$  strain [20, 21, 22, 23, 24, 25, 26] and a distribution of tilts of the easy axes of the molecules [27, 28].

In this paper we present high sensitivity magnetometry and high frequency electron paramagnetic resonance (EPR) experiments carried out on single crystals of  $Mn_{12}$ . These experimental techniques and an in-depth analysis of the implications of the combined data set allow us to determine the symmetry and origin of MQT. We show that variations in the local solvent environments around the  $Mn_{12}O_{12}$  magnetic cores are important to MQT because they lower the symmetry of the core and lead to tilts of the magnetic easy axis. Disorder in the molecule's solvent environment can explain many of the features observed experimentally. This includes non magnetic exponential relaxation, the absence of tunneling selection rules, an unusual Berry phase effect, and multiple and broad EPR absorption peaks.

The article is organized as follows: In Section II we analyze the spin Hamiltonian of  $Mn_{12}$  and discuss the symmetry of MQT expected based on this Hamiltonian. The effect of a disorder induced transverse anisotropy combined with intrinsic transverse anisotropy has interesting consequences of MQT that we explore in depth in this article. In Section III we describe magnetic relaxation measurements carried out in the pure quantum regime, where MQT is without thermal activation [11]. Section IV presents high frequency EPR measurements. In Section V we discuss the implications of our analysis and measurements to the understanding of MQT.

## II. TUNNELING IN $Mn_{12}$ :

$Mn_{12}$  molecules consist of core of four  $Mn^{+4}$  ions ( $S = 3/2$ ) surrounded by a ring of eight  $Mn^{+3}$  ions (spin  $S = 2$ ) (see Fig. 1). These two groups of spins

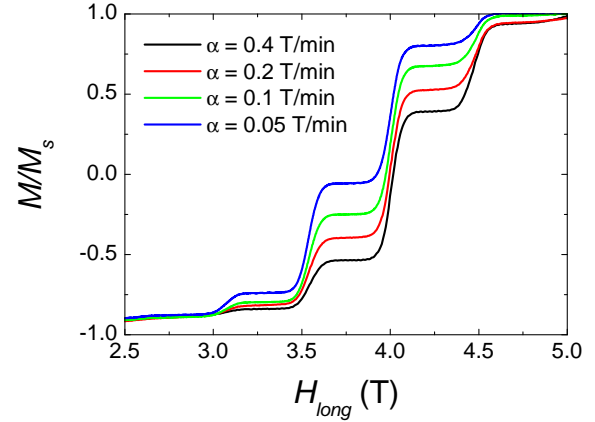


FIG. 2: (Color on-line) Magnetization versus field of a single crystal of  $Mn_{12}$ -acetate SMM for several sweep rates,  $\alpha = dH/dt$ . The measurements have been conducted at  $T = 0.6$  K, in the pure quantum regime [11]. The observed increase of the relaxation at regular spaced field intervals,  $H_k = D + g_B \cdot 0.44$  T, correspond to MQT at resonances  $k = 6; 7; 8; 9$  and 10.

order ferrimagnetically producing a net spin  $S = 10$  ( $8 \cdot 2 + 4 \cdot 3 = 2 = 10$ ) [29, 30, 31].

The spin Hamiltonian of  $[Mn_{12}O_{12}(CH_3COO)_{16}(H_2O)_4] \cdot 2CH_3COOH \cdot 4H_2O$  is given by

$$H = D S_z^2 + B S_z^4 + g_B H S_z \cos \theta + H_T + H_A + H^0; \quad (1)$$

The first two terms represent the uniaxial magnetic anisotropy of the molecule ( $D > 0$  and  $B > 0$ ). The parameters,  $D$  and  $B$ , have been determined by high frequency EPR experiments for the samples studied in this work and will be discussed in greater detail below. Semiclassically this spin Hamiltonian leads to a double potential well, in which opposite projections of the spin on the  $z$ -axis are separated by an anisotropy energy barrier  $D S^2 + B S^4$  (60 K) (see Fig. 1). The third term is the Zeeman energy due to the longitudinal component of an external magnetic field,  $H_z = H \cos \theta$ , where  $\theta$  is the angle between the field and the easy axis of the molecule. A magnetic field applied along the  $z$ -axis shifts the double well potential and the energies of the projections of the magnetization. At certain values of the  $z$ -axis field (resonance fields) the levels  $m$  and  $m^0$  with antiparallel projections on the  $z$ -axis have nearly same energy,  $H_k = kD + g_B = 0.44$  T ( $k = m + m^0$ ) (see Fig. 1).

At these resonances MQT is turned on by interactions that break the axial symmetry and mix the levels  $m$  and  $m^0$ . These off-diagonal terms have different origins: (a) transverse anisotropy terms are included in  $H_A$ , (b)  $H^0$  characterizes the transverse components of magnetic fields due to intermolecular dipolar interactions and hyperfine nuclear fields, and (c)  $H_T$  is the Zeeman interaction associated with the transverse component of the external magnetic field. Off-diagonal terms in the Hamiltonian remove the degeneracy of the spin-levels at the resonances creating an energy difference between symmet-

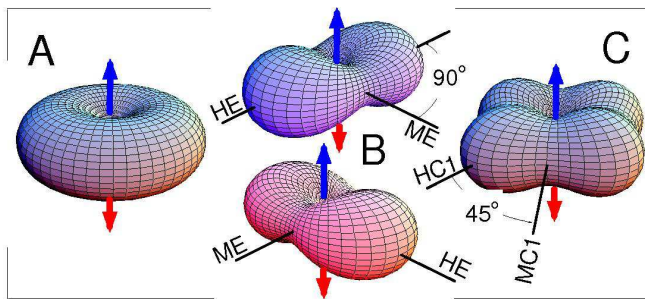


FIG. 3: (Color on-line) 3D representations of the anisotropy barrier. (A) Uniaxial anisotropy barrier in the absence of transverse anisotropy terms. Color arrows represent the preferred orientation of the spin along the z-axis. (B) Anisotropy barriers corresponding to opposite signs of second order anisotropy,  $E(S_x^2 - S_y^2)$ . The lines represent the hard (H) and medium (M) axes which are separated by 90 degrees. A change of the sign of  $E$  corresponds to a rotation of the transverse magnetic axes by 90 degrees. (C) Anisotropy barrier due to fourth order anisotropy,  $C(S_x^4 + S_y^4)$ . In this case there are two hard and two medium transverse axes separated by 45 degrees. A change of the sign of  $C$  produces a 45 degree rotation of the transverse magnetic axes.

ric and antisymmetric superpositions of spin-projections that is known as the tunnel splitting, (see eq. 1).

Figure 2 shows magnetization curves measured at  $T = 0.6$  K for several sweep rates of the longitudinal field,  $\dot{H} = dH/dt$ , of a single crystal of  $Mn_{12}$ -acetate. The abrupt increases of the magnetization toward the equilibrium magnetization are due to MQT at the resonant fields. It is important to note for our discussion that MQT is observed at consecutive resonances and implies the absence of quantum tunneling selection rules. This has important implications for the understanding of MQT because transverse anisotropy terms introduce selection rules (i.e., the only source that allows MQT at odd-resonances ( $k = 1; 3; 5; \dots$ ) is a transverse magnetic field).

#### A. Symmetry of MQT: Transverse Anisotropies and Transverse Magnetic Fields

The tunneling characteristics depend on the form of the off-diagonal terms, which is determined by the structure and defects in the sample (i.e. the molecule site symmetry and any disorder). In this subsection we will examine the consequences of the off-diagonal terms in the Hamiltonian on MQT. We consider both transverse anisotropy terms and transverse magnetic field terms.

The simplest expression for the off-diagonal part,  $H_T$ , of the Hamiltonian of Eq. (1) due to a transverse magnetic field,  $H_T$ , is

$$H_T = g_B H_T (S_x \cos \theta + S_y \sin \theta); \quad (2)$$

This represents the Zeeman energy for a field in the  $xy$ -plane at an angle  $\theta$  with respect to the  $x$ -axis. The

tunnel splitting,  $\Delta_k$ , is very sensitive to the transverse field,  $H_T = \sqrt{H_x^2 + H_y^2}$ . The dependence of  $\Delta_k$  on  $H_T$  for small transverse magnetic fields ( $H_T \ll 2DS = g_B \mu_B$ , the anisotropy field) is given by [5],

$$\Delta_k(H_T) = g_k \frac{g_B H_T}{2DS}^k; \quad (3)$$

where  $g_k = \frac{2D}{[(2S-k)1]^2} \frac{(2S-k)!(2S)!}{k!}$  and  $k = 2S - k$ . The power law dependence of  $\Delta_k$  on  $H_T$  causes the tunnel splitting to vary by many orders of magnitude for transverse fields in the range of a few Tesla. This allows the study of MQT properties of SMMs with a wide range of experimental techniques that go from quasi-static magnetization measurements to high frequency EPR experiments simply by applying different magnitudes of the external transverse field.

In a real system of molecules, internal transverse fields can also play an important role. These fields can arise from intermolecular dipolar or exchange interactions, intramolecular hyperfine fields or tilts of the molecular easy axis, as we discuss below. Without going into detail in the discussion of the origin of these transverse fields (this will be discussed in the experimental part of the paper) we analyze the symmetry imposed by a off-diagonal term in the Hamiltonian due to the presence of both an internal field and an externally applied transverse magnetic field. The magnitude of the tunnel splitting will depend on the vector sum of these fields, leading to different splitting magnitudes for different relative orientations of these fields. We can distinguish between two different situations depending on the internal transverse fields in the sample: a) A uniform transverse field along a particular direction would lead to one maximum in tunnel splitting versus the angle of the external transverse field. When the external field is applied parallel to the internal field the tunnel splitting would be large than when the external field is applied antiparallel to the intrinsic field. b) A more realistic picture has to include the fact that there is a distribution of internal transverse fields in a SMM crystal (i.e. dipolar or hyperfine interactions). If one assumes a random distribution of the orientation of the internal transverse fields, the expected MQT rates are independent of the orientation of an external transverse field. It has been shown through relaxation measurements carried out on  $Mn_{12}$ -BAC that a random orientation-distribution of internal transverse fields can be explained by a distribution of tilts of the easy axes of the molecules when the experiment is done in the presence of a high longitudinal field [8]. Tilts of the easy axes of the molecules have also been seen in  $Mn_{12}$ -acetate by high frequency EPR experiments [27]. In this case, the tilts are related to disorder of the solvent molecules surrounding the magnetic cores and are found to lie in two orthogonal planes.

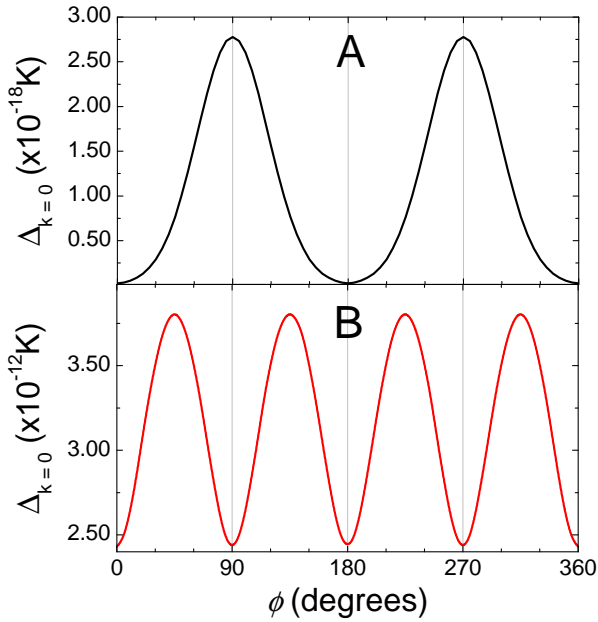


FIG. 4: Tunnel splitting of the ground state, resonance  $k = 0$ , as a function of the orientation of a transverse field of 0.3 T applied in the hard magnetic plane of the molecule for only second (A) and only fourth (B) order anisotropy terms. We have used  $D = 548$  mK,  $B = 1.17$  mK,  $E = 10$  mK and  $C = 0.022$  mK in the Hamiltonian of Eq. (1). The graphic clearly shows the 2-fold and 4-fold symmetries imposed these by different anisotropy terms.

Now we examine the effect of transverse anisotropy terms in the Hamiltonian. Considering only the lowest transverse anisotropy orders that have been observed in SMMs,  $H_A$  has the form

$$H_A = E (S_x^2 - S_y^2) + C (S_+^4 + S_-^4) : \quad (4)$$

The first term is the second order anisotropy which is present in SMMs molecules of rhombic symmetry (i.e.  $\text{Fe}_3$  [33]) and, as it will be shown below, is also present in  $\text{Mn}_{12}$ -Ac due to disorder that lowers the  $S_4$  symmetry of the molecules [16, 18, 19]). The second term is fourth order in the spin operators and is the lowest order anisotropy allowed by the tetragonal symmetry. This form of the transverse anisotropy has been observed in EPR studies of several SMMs of tetragonal symmetry such as,  $\text{Mn}_{12}$ -Ac [19],  $\text{Mn}_{12}$ -B rAc and  $\text{Ni}_4$  [34].

Let us consider in detail the consequences of each transverse anisotropy term. In Fig. 3 we show the shape of the classical anisotropy barrier separating antiparallel orientations of the spin  $z$ -projections (colored arrows). In the absence of transverse terms (Fig. 3A), the anisotropy barrier is determined by the uniaxial anisotropy of the molecules (first and second terms in Hamiltonian of Eq. (1)). These uniaxial anisotropy terms determine a hard anisotropy plane between opposite orientations of the spin states along the easy magnetic  $z$ -axis. Note that this barrier is isotropic in the  $x$ - $y$  plane. In this case, the dependence of the tunnel splitting on an external trans-

verse magnetic field is insensitive to the orientation of the transverse field in the hard plane.

This situation changes in the presence of a transverse anisotropy. Fig. 3B shows how the anisotropy barrier is modified by a second order anisotropy term on the form  $E (S_x^2 - S_y^2)$ . This term introduces one hard and one medium axis in the hard plane (the  $x$ - $y$  plane) that are separated by 90 degrees. That is, for positive  $E$  the  $x$  axis ( $\ell = n$ , with  $n = 0, 1$ ) is hard and  $y$  axis ( $\ell = (2m - 1) = 2$ ), with  $m = 1, 2$ ) is medium. Note that a change of the sign of  $E$  produces a 90 degree rotation of these transverse magnetic axes. In this case, the tunnel splitting,  $\Delta$ , depends on the angle,  $\phi$ , of the applied transverse field,  $H_T$ . A transverse magnetic field applied along the medium axis produces a larger tunnel splitting than the same field applied along the hard axis. This leads to an oscillatory dependence of  $\Delta$  on  $\phi$  with  $2m$  maxima, with the maxima and minima separated by 90 degrees (see Fig. 4A). A second order anisotropy also introduces MQT selection rules. In the absence of a transverse field, this term only allows MQT for resonances that are even (i.e.  $k = 2i$  with  $i = 0; 1; 2; 3; \dots$ ).

Fig. 3C shows the modification of the anisotropy barrier in the presence of a fourth order anisotropy term of the form  $C (S_+^4 + S_-^4)$ . This anisotropy produces two medium and two hard axes in the hard plane. The separation between medium ( $\ell = n = 2$  with  $n = 0; 1; 2; \dots$  for  $C > 0$ ) and hard ( $\ell = (2n + 1) = 4$  with  $n = 0; 1; 2; \dots$  for  $C > 0$ ) axes is 45 degrees. Thus the tunnel splitting will have a 4-fold pattern of oscillations as a function of the angle of a transverse field, with maxima and minima spaced by a 45 degrees (see Fig. 4B). This term introduces a selection rule that allows tunneling transitions from the ground state for resonances that are a multiple of 4 ( $k = 4i$  with  $i = 0; 1; 2; 3; \dots$ ). In Fig. 4 we show the expected behavior of the tunnel splitting of the ground state for resonance  $k = 0$  versus the angle of the applied transverse field,  $H_T = 0.3$  T. The tunnel splitting is calculated using the Hamiltonian of Eq. (1) with  $D = 548$  mK and  $B = 1.17$  mK and considering only second order anisotropy ( $E = 10$  mK, Fig. 4A) and only fourth order anisotropy ( $C = 0.022$  mK, Fig. 4B).

## B. Disorder in the Molecular Environment

Recent experimental results have shown that MQT in  $\text{Mn}_{12}$ -acetate is modulated by off-diagonal terms that are generated by disorder in the vicinity of the molecules. Disorder allows for anisotropy terms that are lower order in the spin-operators than those imposed by the average symmetry of the SMM crystals. Disorder can also lead to tilts of the easy axes from the crystallographic easy axis [9, 10, 17, 18, 19, 27, 28]. The phenomena that have been explained by disorder can be summarized as follows: a) observation of MQT relaxation at  $k$ -resonances that are not allowed by the quantum selection rules imposed by the symmetry of the molecule and b) non-exponential

magnetic relaxation which suggests the existence of a distribution of tunnel splittings.

Two distinct models of disorder have been proposed. Chudnovsky and Garanin [14, 15] proposed that random line dislocations in a crystal lead, via magnetoelastic interactions, to a lower molecule symmetry and a broad distribution of tunneling rates. Subsequent magnetic relaxation experiments indeed showed the existence of a broad distribution of tunneling rates and were analyzed in terms of this model [9, 10]. In contrast, Comia et al. [16] suggested, based on detailed x-ray analysis, that variations in the position of the two hydrogen-bonded acetic acid molecules surrounding the  $M_{n12}$  clusters lead to a discrete set of molecules with lower symmetry than tetragonal. More recent magnetic relaxation experiments [18] and high frequency EPR experiments [19] have confirmed the latter model, showing a 2-fold symmetry of the tunnel splitting as a function of the direction of an external transverse field. These results have naturally been associated with a second order transverse anisotropy that is generated by disorder in the solvent surrounding the  $M_{n12}$  molecules. Moreover, the observation of a distribution of transverse fields in  $M_{n12}$ -BAC [28] and tilts in  $M_{n12}$ -acetate [27] suggests that tilts of the easy axes of the molecules are responsible of the MQT relaxation at odd- $k$  resonances.

The implication of these models of disorder on MQT in  $M_{n12}$ -acetate is as follows. Chudnovsky and Garanin [14, 15] assume a random distribution of edge dislocations with collinear axes to calculate a representative distribution of second order transverse anisotropies. They find: a) the corresponding distribution of tunnel splittings is broad on a logarithmic scale, b) the mode of the distribution is at  $E = 0$ . This leads to a distribution of tunnel splittings with a very long tail to small values of the tunnel splitting. And, c) for small concentrations of dislocations most molecules are far from the dislocation cores and the magnetic axes associated with the transverse anisotropy are oriented randomly. The first point can explain the non-exponential relaxation observed in previous experiments and was recently used to model Landau-Zener relaxation experiments carried out at different sweep rates of a longitudinal magnetic field that crossed several MQT resonances [9]. Also experiments in which a  $M_{n12}$ -acetate single crystal was treated with rapid thermal changes were explained in terms of the dislocation model [10]. In a more recent experimental study, a Landau-Zener method that involved crossing the same resonance several times permitted the study of nearly the whole distribution of tunnel splittings in a  $M_{n12}$ -acetate single crystal in a single resonance [17]. The results obtained were compared to the distribution function proposed by Chudnovsky and Garanin. It turned out that a distribution of second order anisotropies with mode at  $E = 0$  is not able to explain the relaxation data. More recently, both magnetic relaxation and high frequency EPR experiments [18, 19] confirmed the discrete nature of the distribution of transverse anisotropies and, more-

over, the fact that the magnetic axes of the transverse anisotropy is also discretely distributed along particular directions in the hard anisotropy plane of the molecules, contrary to the random distribution expected from the dislocation model. These latter results will be presented in detail in the experimental sections of this paper.

From x-ray diffraction studies Comia et al. [16] showed that the fourfold symmetry of  $M_{n12}$ -acetate molecules is lowered by disorder of the acetic acid molecules (2 molecules with 4 possible sites). This gives rise to a set of six different molecules (4 of them with  $E \neq 0$ ). The fact that the second order anisotropy is generated by disorder in the solvent molecules implies that both the abundance and magnitude of the  $E$  for each isomer could depend on the synthesis process as well as on the solvent losses that a particular crystal experienced prior to measurement. From x-ray data Comia et al. calculated the  $E$  parameters for the different isomers [16]. These should be taken as estimates since the data was from one crystal and the  $E$ -parameters were computed using an empirical model. Nonetheless, this model represents an important step in the understanding of MQT in  $M_{n12}$ -acetate.

The relevant points of the solvent disorder model can be summarized as follows: a) there is a discrete set of  $E$  values in a sample. This means that the distribution of tunnel splittings is a discrete function with peaks at several  $E \neq 0$  values. b) There are equal populations of isomers having opposite signs of the second order anisotropy  $E$ . This means that the medium and hard axes associated with each  $E$  value will be discretely distributed over the hard plane of the crystal with a separation of 90 degrees. And c) the hard anisotropy axes of the second order anisotropy are rotated by 30 degrees from the anisotropy axes corresponding to the fourth order anisotropy. The first point has been confirmed by high frequency EPR experiments by the observation of discrete peaks in the absorption spectra that correspond to different discrete  $E$  values and have the angular dependence expected from this model [19]. The second point has been confirmed through magnetic relaxation measurements in which a portion of molecules having different signs of  $E$  have been studied [17]. The third point has important implications on MQT, that will be discussed below. We note that both models suggest the presence of tilts of the easy magnetic axes of the molecules.

### C. The Effect of Disorder on MQT

In this section we will present model calculations of the dependence of the tunnel splitting on the angle and the magnitude of an external transverse field taking into account the presence of both second and fourth order anisotropies. These terms must be considered on an equal footing because they produce comparable tunnel splittings. This is seen as follows. In perturbation theory the splitting between levels  $m$  and  $m^0$  associated with the second order anisotropy is approximately

$E$   $D$  ( $E=2D$ )<sup>(m<sup>0</sup>m)=2</sup>, while that associated with the fourth order anisotropy is  $C$   $D$  ( $C=2D$ )<sup>(m<sup>0</sup>m)=4</sup>. Thus, provided  $E^2$   $D$   $C$  these are comparable in magnitude, independent of  $m$  and  $m^0$ . This is the case for  $Mn_{12}$ -ac, as  $E = 10^2$  K,  $C = 10^5$  K and  $D = 1$  K. For this reason there is an intricate interplay between these anisotropy terms that also occurs over a broad range of transverse magnetic fields, and can thus be probed both in EPR and MQT studies.

In  $Mn_{12}$ -ac these transverse anisotropy terms have a different origin. The fourth order transverse anisotropy term is imposed by the symmetry of the molecule, while a magnitude-distributed second order term, with equal population of opposite signs, is generated by a distribution of micro-environments of the magnetic molecules. However, there is no reason to assume that these anisotropies are collinear since they come from different sources; one is associated with the ideal  $S_4$  symmetry, the other is disorder induced and lowers this symmetry. Therefore, we will take into account an misalignment,  $\beta$ , between the magnetic axes associated with each transverse anisotropy term.

We write the transverse anisotropy part,  $H_A$ , of the Hamiltonian (Eq. (4)) in the following form

$$E(e_1(S_x^2 - S_y^2) + e_2(S_x S_y + S_y S_x)) + C(S_+^4 + S_-^4); \quad (5)$$

where,

$$e_1 = (\cos^2 \beta - \sin^2 \beta) \quad e_2 = 2\cos \beta \sin \beta; \quad (6)$$

This introduces an angle  $\beta$  between hard axes of second and fourth anisotropy terms (see Fig. 5), the  $E$  and  $C$  terms respectively.

First we consider two angles,  $\beta$ , with  $C > 0$  and  $E > 0$ . a)  $\beta = 0$ : the hard axis of  $E$  (HE) is in the same direction of one of the hard axes of  $C$  (HC1) and orthogonal to the other hard axis (HC2). The latter (HC2) is parallel to the medium axis of  $E$  (ME), so  $HE=HC1$  and  $ME=HC2$ . b)  $\beta = 45^\circ$  HE is 45 degrees from both HC1 and HC2 axes. In this case HE is in the same direction as one of the medium axes of  $C$  (MC1) and ME is along MC2, so  $HE=MC1$  and  $ME=MC2$ . Note that there are equivalent values of the misalignment angle  $\beta = i90$  and  $\beta = (2i+1)45$  for  $i=0;1;2;3$ .

In the next subsections we will show the effect of having a misalignment on the symmetry of MQT and on the transverse field dependence of the tunnel splitting for different orientations of the applied field. The calculations have been done for parameters and conditions close to those shown in the experimental sections of this article. In the following we consider in some detail the consequences of the solvent disorder model as this model can adequately explain many of our experimental observations.

As mentioned, one of the important consequences of the solvent disorder model is the fact that there must be equal populations of molecules having opposite signs of  $E$ . This is because on average crystals of  $Mn_{12}$ -acetate

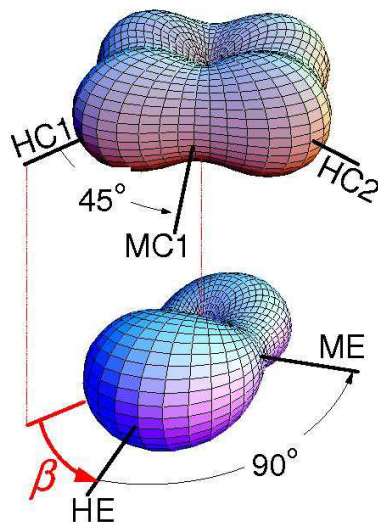


FIG. 5: (Color on-line) 3-D representation of the anisotropy barriers corresponding to fourth (upper graph) and second order (lower graph) anisotropies with an angle  $\beta$  between the corresponding hard axes.

have tetragonal symmetry. Note that Fig. 5 represents the picture for the molecules having  $E > 0$ . Thus there will be molecules in the sample with the magnetic axes of  $E$  rotated by 90 degrees respect to those represented in Fig. 5.

#### 1. Effect of Disorder on MQT Symmetry

We begin by considering those molecules with  $E > 0$ , in the presence of large transverse field, as this field corresponds to that used in high frequency EPR experiments (section IV). Fig. 6 shows the behavior of the ground state tunnel splitting,  $\nu_{10;10}$  (resonance  $k=0$ ), versus the angle,  $\beta$ , of an external transverse field of 9 Tesla. The calculations have been done for  $\beta = 0$ ,  $D = 548$  mK,  $B = 1.17$  mK,  $C = 0.022$  mK and different values of  $E$ .

One interesting result in this figure is the observation of fourfold pattern of maxima imposed by the fourth order anisotropy. There are four maxima of  $\nu_{10;10}$  that occur very close to the medium axes of  $C$  for small values of  $E$ . Only when  $E$  becomes very large do the maxima move towards the medium axis of  $E$  to give, at high enough  $E$ -values ( $E \gg 20$  mK), a twofold pattern of maxima. However, for the parameters estimated with the solvent disorder model,  $E < 10$ – $15$  mK, the tunnel splitting is expected to show fourfold maxima in the direction of the medium axes of  $C$ .

Fig. 7a shows the behavior of the ground tunnel splitting,  $\nu_{k=0}$ , for the same conditions of Fig. 6, that is for  $\beta = 0$ , but taking into account the equal population of molecules having opposite signs of  $E$ . In this case we have used  $E = E_{av} = 3$  mK. The modulation of the fourfold symmetry by  $E$  is opposite for different signs of

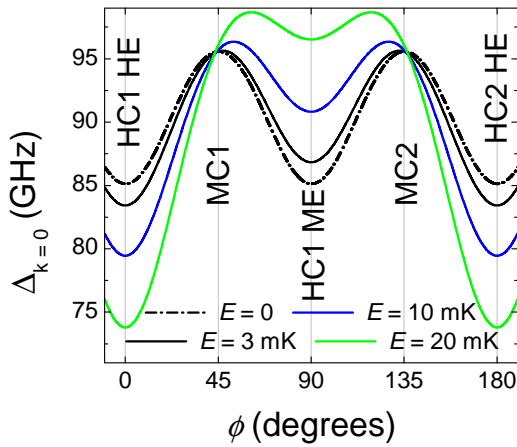


FIG. 6: (Color on-line) Behavior of the ground splitting,  $\Delta_{k=0}$ , versus the angle of orientation of a transverse field,  $H_T = 9 T$ , for  $\beta = 0$  and different values of  $E > 0$ .

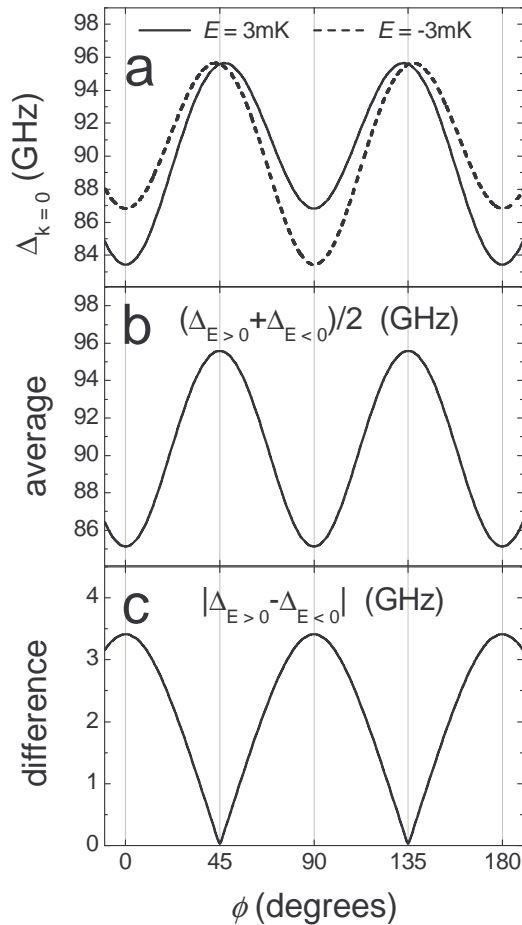


FIG. 7: (a) Ground tunnel splitting,  $\Delta_{k=0}$ , versus the angle or orientation of a transverse field,  $H_T = 9 T$ , for  $\beta = 0$  and  $E = +3 \text{ mK}$  (solid line) and  $E = -3 \text{ mK}$  (dashed line). (b) Average value of the tunnel splitting assuming both  $E$ -signs. (c) Difference between the tunnel splitting values of  $E > 0$  and  $E < 0$ .

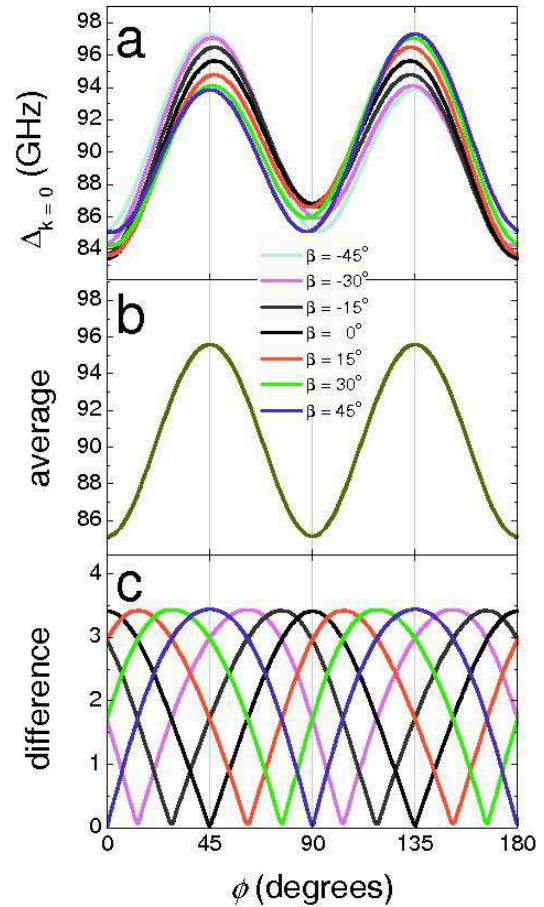


FIG. 8: (Color on-line) (a) Ground tunnel splitting,  $\Delta_{k=0}$ , versus the angle of a transverse field,  $H_T = 9 T$ , for  $E = +3 \text{ mK}$  and different values of  $\beta$ . (b) Average value of the tunnel splitting assuming both  $E$ -signs for each value of  $\beta$ . All the curves are in the same curve. (c) Difference between the tunnel splitting values of  $E > 0$  and  $E < 0$  for different  $\beta$ -values.

$E$ . However, the maxima are approximately at the same position independent of the sign of  $E$ . In Fig. 7b we show the average value of the tunnel splitting calculated as  $(\Delta_{E>0} + \Delta_{E<0})/2$ . This average shows a symmetric four-fold rotation pattern, the same that would be generated by only a fourth order anisotropy. Therefore a measurement of the average tunnel splitting of a crystal cannot distinguish between second and fourth order transverse anisotropies if there are equal populations of molecules with opposite signs of  $E$ .

The absolute difference between the tunnel splittings corresponding to opposite signs of  $E$  is shown in Fig. 7c. In this case,  $\beta = 0$ , the difference is maximal along the hard axes of  $C$  and vanishes along the medium axes of  $C$ . Importantly, this provides a means of inferring the presence of a second-order anisotropy through an appropriate experiment (this will be shown below and in section IV).

We now consider the effect of a misalignment,  $\beta \neq 0$ , on the previous calculations. Fig. 8a shows the behavior of the ground tunnel splitting,  $\Delta_{k=0}$ , versus the angle of

the applied transverse field,  $H_T = 9 \text{ T}$  for  $E = 3 \text{ mK}$  and different values of  $\beta$ , from  $\beta = 45^\circ$  to  $\beta = -45^\circ$  in increments of 15 degrees. Note that the black line,  $\beta = 0$ , is the result presented in Fig. 7a. A misalignment  $\epsilon \neq 0$  generates an asymmetry between the maxima of the tunnel splitting. For example, for  $\beta = 45^\circ$ , the maximum at  $\phi = 45^\circ$  is bigger than the maximum at  $\phi = 135^\circ$ . Note that the hard axis of E (HE) for this value of  $\beta$  is  $\phi = 45 + n180$  ( $n = 1, 2, \dots$ ) while the medium axis (ME) is along  $\phi = 45 + n180$ . In general, even though the ME axis is at  $\phi = \beta + (2n+1)90$  (with  $n = 0, 1, \dots$ ), the maxima of the tunnel splitting are in the direction of the medium axes of C. The second order anisotropy introduces an asymmetric modulation of the maxima and minima of the tunnel splittings that depends on the value and the sign of  $E$  and on the misalignment angle  $\epsilon$ .

Fig. 8b shows that the average value of the tunnel splitting is independent of the angle of misalignment and has four maxima. All the results collapse in the same curve. So again a direct measurement of the average value of  $\Delta_{k=6}$  would not give information about the misalignment between these anisotropies.

Fig. 8c shows the difference between  $E > 0$  and  $E < 0$  for the same parameters used in the previous calculation and different values of  $\beta$  from  $45^\circ$  to  $-45^\circ$ . This difference has again four maxima for all the angles  $\beta$ , as in the case of  $\beta = 0$ . However, the position of the maxima is different for different values. In fact, the position of the maxima depends directly on the value of  $\beta$  as  $\phi_{\text{max}} = \beta + n90$  ( $n = 0, 1, 2, \dots$ ). Consequently, a measurement of this difference would not only provide the value of  $E$  but also give the angle of misalignment between second and fourth order transverse anisotropies.

We thus note that within the solvent disorder model the ground tunnel splitting of resonance  $k = 0$  at high transverse field values will show a fourfold rotation pattern with respect to the angle of orientation of the applied field. This symmetry is modulated by the second order anisotropy. However, equal populations of molecules with opposite signs of  $E$  will give an average tunnel splitting with four maxima that is indistinguishable from that corresponding fourth order transverse anisotropy. The only way to determine the presence of second order anisotropy is by examining the difference of the tunnel splittings corresponding to molecules with opposite signs of  $E$ . The latter would give the value of  $E$  and the misalignment angle between the second and fourth order anisotropies. We will show how such a measurement is possible in the experimental part of the paper.

Let us now consider the situation relevant to understanding the physics of MQT in magnetic studies in which much smaller tunnel splittings are probed ( $10^6 \text{ K}$ ). We will analyze the behavior of the splitting for resonance  $k = 6$  ( $m = 10, m^0 = 4$ ) versus the angle,  $\phi$ , of a small external transverse field. The calculation has been done with the same D, B and C parameters of the

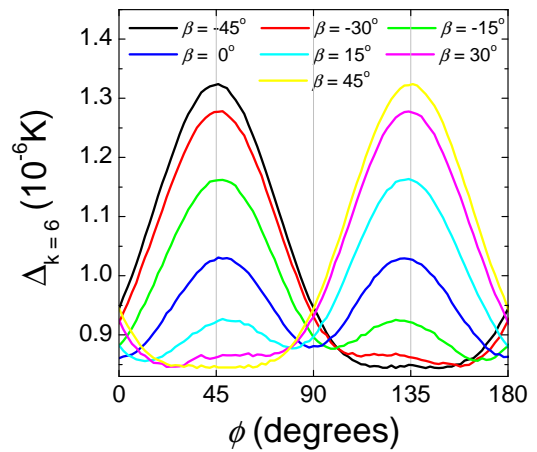


FIG. 9: (Color on-line) Ground tunnel splitting,  $\Delta_{k=6}$ , versus angle of a transverse field,  $H_T = 0.35 \text{ T}$ , for  $E = +3 \text{ mK}$  and different values of  $\beta$ .

Hamiltonian as those of the previous calculations. We have used  $E_j = E_{\text{av}} = 3 \text{ mK}$  and a transverse magnetic field,  $H_T = 0.35 \text{ T}$ , which corresponds to the situation studied in the dc Landau-Zener relaxation experiments that will be presented in section III.

The results are shown in Fig. 9. This situation is substantially different from that of previous case of resonance  $k = 0$ . The tunnel splitting has a pattern that goes from two-fold maxima for  $\beta = 45^\circ$  to four-fold maxima for  $\beta = 0$ . Interestingly, the maxima are in the directions of the medium axes of C independent of the direction of the medium axis of E. For example, for  $\beta = 30^\circ$  the two maxima of the tunnel splitting are at  $\phi_{\text{max}} = 45 + n90 = 45; 135$  (with  $n = 0$  and 1) while the directions of the medium axis of E are  $\phi_{\text{ME}} = \beta + 90 = 60; 240$ . So for some  $\beta$ -values the tunnel splitting exhibits a twofold pattern of maxima with position determined by the fourth order anisotropy. We have done these calculations for bigger values of  $E$  (not shown in this paper) that indicate that the range of  $\beta$ -values around  $\beta = 0$  that exhibits fourfold symmetry is narrower the bigger the value of  $E$ . However, for  $E$ -values smaller than  $30 \text{ mK}$  the maxima positions still are determined by the fourth order anisotropy. This fact constitutes an unexpected result in a system with second and fourth order anisotropies that is first pointed out in this work and has important consequences for the interpretation of the experimental measurements that have been previously published by some of the authors of this work [18, 19], as will be explained in the experimental sections III and IV.

We have calculated the average value of the tunnel splitting for different angles assuming an equal population of molecules with different signs of  $E$ . The results are shown in Fig. 10. For all values of  $\beta$  there is clearly a fourfold rotation pattern of the average tunnel splitting with symmetric maxima and minima along directions determined by the fourth order anisotropy. A gain, the only

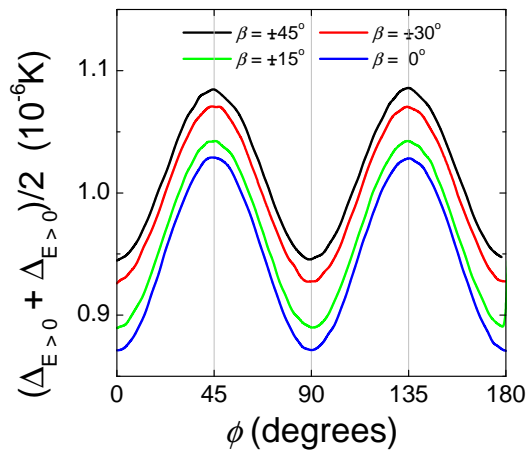


FIG . 10: (Color on-line) A verage value of the ground tunnel splitting,  $\nu_{k=6}$ , for opposite signs of  $E$  ( $E = 3\text{jm K}$ ) versus the angle or orientation of a transverse eld,  $H_T = 0.35\text{ T}$ , for di erent values of  $\beta$ .

method to determine the  $E$  value and the relative orientation between  $C$  and  $E$ ,  $\beta$ , is by an appropriate selection of a subset of  $m$  molecules having only one sign of  $E$ . In the latter case, depending on the value of  $\beta$  there is a possibility that the  $m$  molecules selected will also show fourfold symmetry (e.g.  $\beta = 0$ ). It would then not be possible to conclude that such  $m$  molecules have a second order anisotropy. As we will show in sections III and IV this is not the case experimentally. We will show that a selection of a subset of  $m$  molecules with one sign of  $E$  shows twofold symmetry which indicates that the angle of misalignment is close to  $\beta = 45$  (concretely,  $\beta = 30$ ).

## 2. Disorder and the Behavior of the Tunnel Splitting with a Transverse Field: Berry phase

Quantum phase interference is one of the most important phenomena observed in SMMs. Interference effects (Berry phase) in MQT were first discovered by Loss [36] and calculated for a nanomagnet with a biaxial anisotropy by Garg [37]. This phenomenon is due to interference of the quantum tunneling trajectories of the magnetization and has been clearly observed in two SMMs to date [33, 38]. The first observation of the Berry phase was by Wernsdorfer and Sessoli [33] in the SMM  $\text{Fe}_8$ .  $\text{Fe}_8$  has second and fourth order transverse anisotropy. The observation of quantum oscillations was done by applying a transverse eld along the direction of the hard axis of the second order anisotropy (HE), which in this case,  $\phi = 0$ , corresponds to the direction of one of the hard axis of the fourth anisotropy term. We show in Fig. 11 the dependence of the tunnel splitting of resonance  $k = 0$  on the magnitude of an external eld applied along  $\phi = 0$  (hard E anisotropy axis) and  $\phi = 90$  (medium E anisotropy axis). We have used the parameters given in

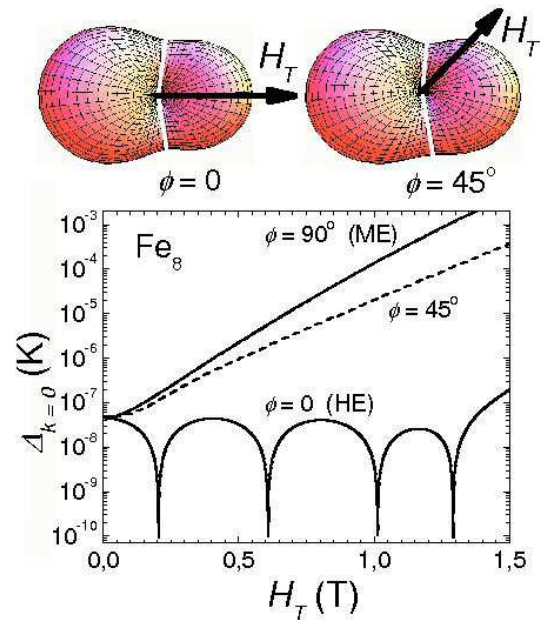


FIG . 11: (Color on-line)  $\text{Fe}_8$  ground tunnel splitting,  $\nu_{k=0}$ , versus the magnitude of a transverse eld applied along the hard (HE) and the medium (ME) anisotropy axes. The parameters used in this calculation were taken from reference [33]. The drawings at the top represent the  $x-y$  plane projections of the anisotropy barrier of  $\text{Fe}_8$  in the presence of a transverse eld applied at different angles. The white lines show two hypothetical quantum tunneling trajectories. When  $H_T$  is applied along the hard anisotropy axis,  $\phi = 0$ , the barrier remains symmetric with respect to the eld. In this case the trajectories interfere. For transverse elds not aligned with the hard axis the asymmetrical distortion of the barrier leads to non-equivalent trajectories, destroying the interference.

reference [33].

The eld spacing between quantum tunneling oscillations of Fig. 11 can be described in terms of the anisotropy parameters  $D$  and  $E$  of the Hamiltonian using a semiclassical approach [37],

$$H = \frac{2k_B}{g_B} P \frac{1}{2E(E+D)}; \quad (7)$$

This is  $0.23\text{ T}$  for  $\text{Fe}_8$  which is smaller than the spacing resulting from the exact diagonalization of the Hamiltonian including fourth order transverse anisotropy,  $H = 0.41\text{ T}$ , and was observed in reference [33]. The reason for this is that the approximation only takes into account the presence of second order anisotropy. Note that the authors of ref. [33] assumed collinear anisotropies to fit the data, thus the angle between HE and HCl axes is  $\beta = 0$  (see Fig. 5). We also have used collinear second and fourth order anisotropy terms in the calculated data shown in Fig. 11. So we can see that the effect of having a fourth order anisotropy that is collinear with a second order anisotropy,  $\beta = 0$ , only modifies the pattern of oscillations but not their structure and shape. Quantum tunneling oscillations were also observed in  $[\text{Mn}_{12}]^{2+}$

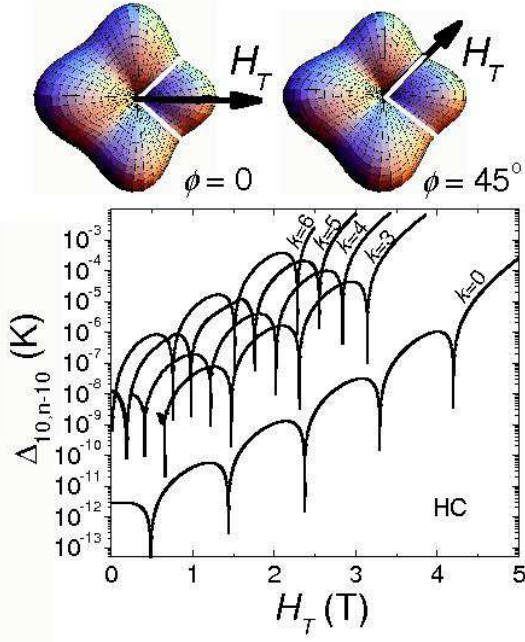


FIG. 12: (Color on-line) Transverse field dependence of  $M n_2$  tunnel splittings of several resonances assuming only fourth order anisotropy. The transverse field is applied along one of the hard axes of C (HC). The drawings at the top of the figure show the distortion of the anisotropy barrier due to a transverse field applied at different angles with respect to the hard axis of the fourth order anisotropy. White lines represent different tunneling trajectories.

which only has a second order transverse anisotropy [38]. In this case, the spacing between oscillations was exactly explained by Eq. (5).

A detailed study of quantum tunneling oscillations in a system with only fourth order transverse anisotropy was theoretically carried out by Park and Garg [39] using the Hamiltonian of  $M n_{12}$ -acetate (Eq. (1)). We show in Fig. 12 calculations of the tunnel splitting of different resonances by using the Hamiltonian of eq. 1 with  $D = 556$  mK,  $B = 1.1$  mK and  $C = 0.03$  mK.

In order to take into account the effect of a misalignment,  $\epsilon \neq 0$ , between second and fourth order anisotropies we have calculated the dependence of the ground tunnel splitting on the magnitude of an external transverse field applied along different characteristic directions in the hard plane of a molecule. For this we have used  $\epsilon = 30^\circ$ ,  $D = 548$  mK,  $B = 1.17$  mK and  $C = 0.022$  mK and different values of  $E > 0$ . For clarity, this situation corresponds to have the following directions for the characteristic transverse anisotropy axes of both anisotropies:  $H_C = 0 + n90 = 0; 90; 180; 270$ ,  $H_{MC} = 45 + n90 = 45; 135; 215; 305$ ,  $H_E = 30 + n180 = 30; 150$  and  $H_{ME} = 30 + (2n - 1)90 = 60; 240$ .

Looking at the result corresponding to  $\epsilon = 30^\circ$  in Fig. 9 (red curve) one can see that the tunnel splitting has twofold symmetry with maxima at  $\epsilon = 45 + n180 = 45; 225$  and minima at  $\epsilon = 135 + n180 =$

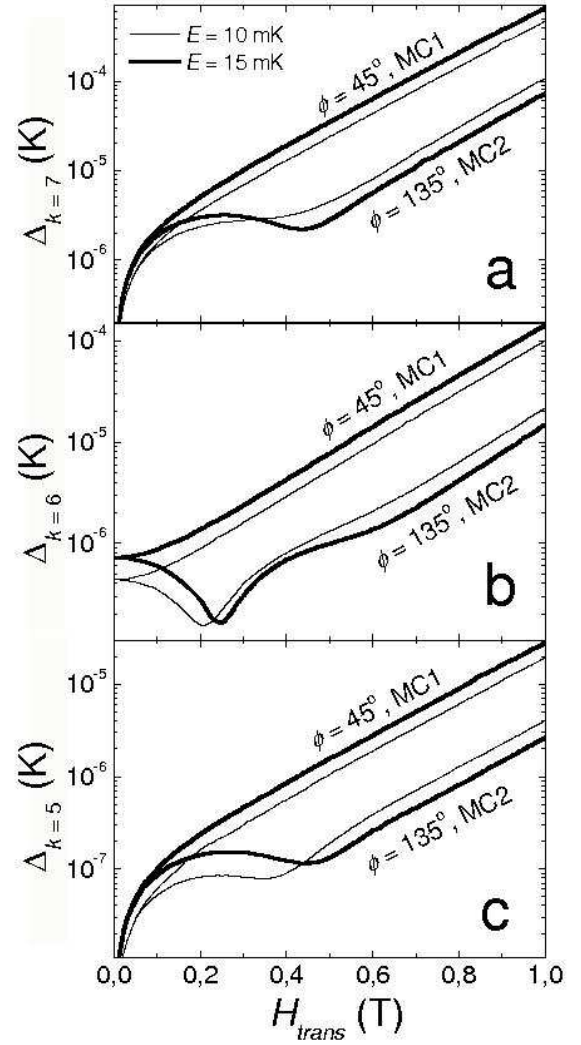


FIG. 13: Transverse field dependence of  $M n_2$  ground tunnel splitting of resonances  $k = 5, k = 6$  and  $k = 7$  for  $E = 10$  mK and  $E = 15$  mK. The transverse field is applied along  $\epsilon = 45^\circ$  and  $\epsilon = 135^\circ$ , which correspond to the positions of the maximum and minimum of  $\epsilon$  for a misalignment  $\epsilon = 30^\circ$ .

$135; 315$ . These directions correspond to the position of the medium axes of C (MC1 and MC2). We have thus calculated the dependence of the ground tunnel splitting for resonances  $k = 5, 6$  and  $7$ . These are shown in Fig. 13a, 13b and 13c respectively, for a transverse field applied along  $\epsilon = 45^\circ$  (tunnel splitting maximum, MC1 axis) and  $\epsilon = 135^\circ$  (tunnel splitting minimum, MC2 axis) using  $E = 10$  mK (thin lines) and  $E = 15$  mK (thick lines).

The results show a very different structure and shape of the Berry phase oscillations in comparison to the case when both anisotropies are collinear. Note that the orientations we used for the applied transverse field correspond to the medium axes of the fourth order anisotropy where one does not expect to have Berry phase oscillations. Moreover, these two orientations,  $\epsilon = 45^\circ$  and  $\epsilon = 135^\circ$ , do not coincide with the hard axis of the

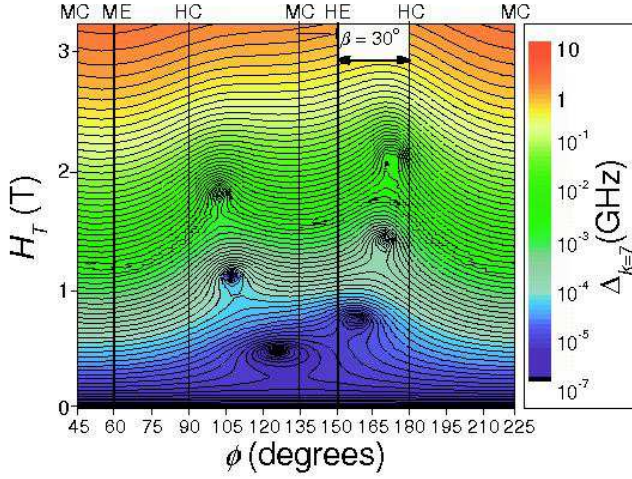


FIG. 14: (Color on-line) Color contour plot of the transverse field dependence of the ground state tunnel splitting of resonance  $k = 7$  for different angles  $\phi$  for a misalignment,  $\beta = 30^\circ$ , between the hard anisotropy axes of E and C. The vertical lines represent the orientations of hard and medium axes of second and fourth order anisotropy terms. This misalignment generates a new and interesting pattern of Berry phase zeros that does not correspond to any of the anisotropies separately.

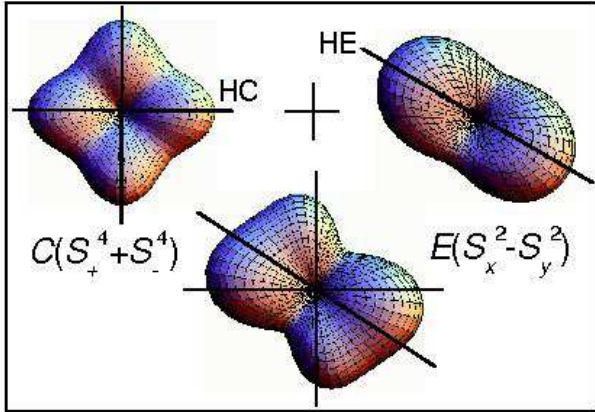


FIG. 15: (Color on-line) Projection of the anisotropy barrier on the  $x-y$  plane for second (right-upper graphic) and fourth (left-upper graphic) order transverse anisotropy terms. The addition of both anisotropies leads to an asymmetric barrier (lower graphic) that makes difficult to see the orientations of a transverse field that would generate equivalent quantum tunneling trajectories and, therefore, Berry phase phenomena.

second order anisotropy, which for  $\beta = 30^\circ$  is along  $\phi = 30^\circ + n180^\circ$ .

In order to have a more complete picture of the effect of the presence of second and fourth anisotropies with non-collinear axes on the Berry phase phenomena we have calculated the dependence of the ground state tunnel splitting of resonance  $k = 7$  on the magnitude of a transverse field applied at different angles, from  $\phi = 45^\circ$  (which correspond to one of the medium axes of C) to  $\phi = 225^\circ$  (which correspond to the opposite orientation of the field along the same hard C-axis). The results

are shown in a color contour plot in Fig. 14. The first thing to point out is that there still are complete zeros of the tunnel splittings in this situation. However, the most significant fact is that these zeros do not appear at any characteristic axis of the transverse anisotropies. Moreover, the structure, shape and position of the zeros are completely independent of the Berry phase corresponding to each anisotropy term separately. Note that the calculations shown in Fig. 13 correspond to transverse fields applied along  $\phi = 45^\circ$  and  $135^\circ$  which correspond to the directions of the maximum and minimum values of the tunnel splitting of Fig. 9 respectively. In the case of  $\phi = 135^\circ$  the tunnel splitting is close to one of the zeros ( $\phi = 125^\circ$  and  $H_T = 0.4$  T in Fig. 14) but far from all the others, explaining the observation of only one and not complete oscillations in Fig. 13a. This new and particular structure of the Berry phase zeros can be better understood looking at the graphic representation of the anisotropy barrier of Fig. 15. The addition of second (right-up in Fig. 15) and fourth (left-up) order transverse anisotropies in a SMM leads to an asymmetric barrier (center-down) where symmetry does not permit a direct identification of the field that generates equivalent quantum tunneling trajectories that can interfere.

From the results we can conclude that the combination of two non collinear and different order anisotropy terms in the spin-Hamiltonian can lead to an interesting situation in which the resulting magnetic response does not depend in any simple way on the form of either anisotropy term separately. In the case we have examined,  $\beta = 30^\circ$ , the hard anisotropy plane has one hard axis along  $\phi = 135^\circ + n180^\circ$ , for which the tunnel splitting is minimum for a given field value. This resulting hard axis, leads to a Berry phase phenomena for the tunnel splittings when a transverse field is applied along this direction. However, these quantum oscillations do not lead to zeros in the tunnel splitting. The shape and position of the oscillations depend strongly on the values of the parameters of the Hamiltonian, especially on the value of E. One can see in Fig. 13 how the minimum move to higher field values and become deeper as E becomes larger. We have shown the results for  $E = 10$  mK and  $E = 15$  mK because they are within the range of values that can explain the experimental results we will present in sections III and IV.

### III. MAGNETIC RELAXATION EXPERIMENTS

We have carried out magnetic relaxation measurements in a single crystal of deuterated  $Mn_{12}$ -acetate SMM in the pure quantum regime ( $T = 0.6$  K) in which relaxation is by MQT without thermal activation over the anisotropy barrier [11]. Deuterated crystals were studied because the purity of the chemicals used in the synthesis leads to very high quality crystals [41].

We have used a high sensitivity micro-Hall effect mag-

netometer [40] to measure the magnetic response of a  $Mn_{12}$ -acetate single crystal of 100 micrometer size and needle shape. We measure the longitudinal component of the magnetization of the sample (z-component) by placing the crystal with one of its faces parallel to the sensor plane and one end just over the cross point of the micro-Hall sensor. The magnetometer was placed inside a low temperature  $He^3$  system. A superconducting vector field magnet was used to apply high magnetic fields at arbitrary directions respect to the crystal axis.

#### A. Landau-Zener Method

The Landau-Zener (LZ) method has been used to study quantum tunneling splittings in SMMs [33] and has become a powerful tool to check for distributions of dipolar and nuclear interactions [38], molecular micro-environments [9, 10, 17, 18] or internal transverse magnetic fields [28] in these materials. The method consists in crossing a MQT resonance by sweeping the longitudinal magnetic field at a constant rate,  $\dot{H} = dH/dt$ , and measuring the fractional change of the magnetization in the process. The anti-crossing of the spin levels  $m$  and  $m^0$  of resonance  $k = m + m^0$  is shown in the inset of Fig. 16. For an ideal system of non-interacting and mono-disperse SMMs and for low enough temperatures (where thermal relaxation is negligible), the normalized change of magnetization,  $(M_{\text{before}} - M_{\text{after}}) = (M_{\text{before}} - M_{\text{eq}})$ , is related to the probability for a molecule to reverse its magnetization by quantum tunneling. The bigger the MQT probability the larger the magnetization change will be. This MQT probability is related to the tunnel splitting,  $\Delta$ , by the LZ formula [42],

$$P_{LZ} = 1 - \exp\left(-\frac{\Delta^2}{2\dot{H}}\right); \quad (8)$$

where  $\dot{H} = g_B(2S - k)$  and  $\dot{H}_0$  is the energy sweep rate.  $R_{LZ} = 1 - P_{LZ}$  is the probability for a molecule to remain in the metastable state  $|j, m^0\rangle$  after crossing the resonance.

It is important to note that this relation is only valid if the internal energy sweep rate a single molecule experiences is proportional to the external sweep rate of the magnetic field. This is not satisfied if there are internal dipolar or nuclear fields. In fact, it has been shown in  $Fe_8$  [38] and  $Mn_{12}$ -acetate [17] that changing dipolar fields lead to deviations from the LZ formula. In order to avoid these effects the external sweep rate must be fast enough to have small magnetization change (i.e. small changes of dipolar fields) in the crossing process. The critical lower value of the magnetic field sweep rate,  $\dot{H}_c$ , that is needed to avoid this situation has been determined to be  $10^3$  T/s for  $Mn_{12}$ -acetate [17]. Due to this, all the experiments presented in this section have been conducted with  $\dot{H} > \dot{H}_c$ .

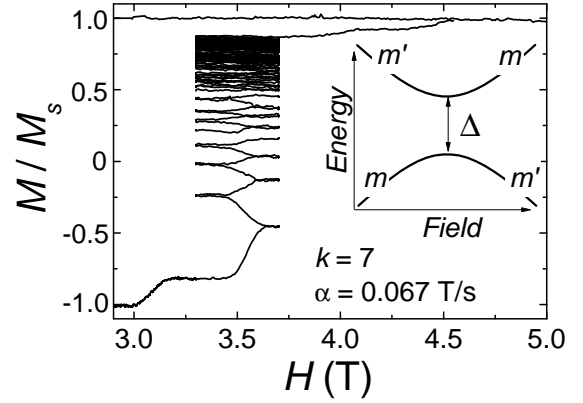


FIG. 16: Landau-Zener multi-crossing relaxation in a  $Mn_{12}$ -acetate single crystal measured at  $T = 0.6$  K by sweeping the longitudinal magnetic field at a constant rate,  $\dot{H} = 6.6 \cdot 10^3$  T/s, multiple times across resonance  $k = 7$ . The inset shows a representation of the energy levels,  $m$  and  $m^0$ , at the anti-crossing point.

#### B. Multi-crossing Landau-Zener Measurements

When there is a distribution of quantum splittings in the sample each molecule has a different MQT probability and the relaxation of the magnetization should reflect this fact. In this case, the MQT probability depends on the distribution of tunnel splittings of the molecules that are in the metastable well before crossing a resonance. After a crossing of a resonance those molecules with the largest tunnel splitting values and, consequently, the highest MQT probability will represent the maximum contribution to the fractional change of the magnetization. Correspondingly, those molecules with smaller tunnel splitting values will remain in the metastable well. Due to this the LZ relaxation method can be used to determine the distribution of tunnel splittings in a sample and to select different parts of the distribution for independent study, as we will show in subsection III.C.

In order to extract the complete distribution of tunnel splittings in  $Mn_{12}$ -acetate we have used a modification of the LZ method that consists of crossing a resonance multiple times, with increasing and decreasing fields. As we said before, in a given crossing,  $n$ , of a resonance molecules with highest tunnel splitting values will relax. Only those molecules with a (exponentially) larger probability that remained in the metastable well can contribute to the relaxation in a second crossing of the same resonance. For  $k > 0$  the molecules that make transitions relax to the stable state,  $m = -S$ , and no longer will exhibit dynamics in subsequent crossings of the same resonance. The repetition of this procedure several times allows determination of the distribution of tunnel splittings in the sample. We show an example of this multi-crossing LZ procedure for resonance  $k = 7$  in Fig. 16.

In a multi-crossing LZ measurement the probability to remain in the metastable well after crossing a resonance

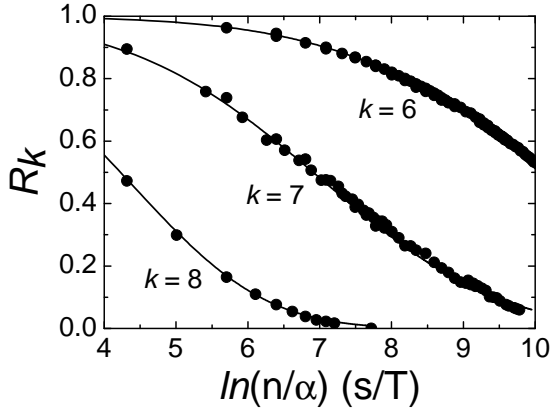


FIG. 17: Landau-Zener probability to remain in the metastable well in multi-crossing relaxations of resonances  $k = 6, 7$  and  $8$  using different sweep rates ( $3.33 \cdot 10^3$  to  $1.33 \cdot 10^2$ ). All the measurements were done beginning with saturation magnetization at  $T = 0.6$  K.

ntimes is given by,

$$R_{LZn} = \exp \left[ -\frac{2}{\pi} \frac{1}{v_{eff}} \right]; \quad (9)$$

where  $v_{eff} = \dot{\omega}n$ . If this expression describes the physics, then relaxation curves recorded at different sweep rates should scale when plotted as a function of the effective sweep rate. This can be clearly observed in Fig. 17, where we show LZ multi-crossing relaxation measurements of resonances  $k = 6, 7$  and  $8$ , carried out at different sweep rates  $\dot{\omega}_c$  ( $3.33 \cdot 10^3$  to  $1.33 \cdot 10^2$ ). Small differences in the results were observed in three different crystals that were synthesized in the same way. These results clearly show that the MQT relaxation rate is not exponential and indicate the presence of a distribution of tunnel splittings within the sample. These results confirm previous experimental observations of non exponential time relaxation in  $Mn_{12}$ -acetate [6, 8, 9, 10]. Moreover, the large fraction of the relaxation that we are able to observe with this method gives direct information on the width of the distribution of tunnel splittings.

We have assumed a log-normal distribution of tunnel splittings to explain our observations. We take the form,

$$f(x) = A \exp \left[ -\frac{(x - x_c)^2}{2\sigma^2} \right]; \quad (10)$$

where  $x = \log(\Delta)$  and  $x_c = \log(\Delta_c)$ .  $\Delta_c$  and  $\sigma$  are the center and the width of the distribution, respectively. The fit of the relaxation curves that are shown in Fig. 17 (solid lines) have been obtained by using,

$$R(\dot{\omega}; n) = \int_{-\infty}^{\infty} R_{LZ}(\dot{\omega}; n) f(\log(\Delta)) d\log(\Delta); \quad (11)$$

with  $x_c$  and  $\sigma$  as free parameters in the fit procedure. The resulting curves are in excellent accord with the

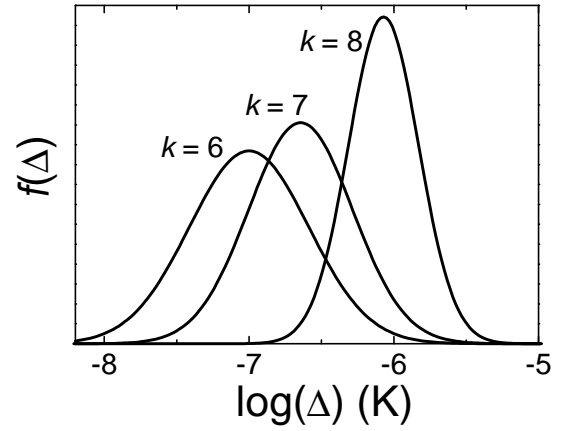


FIG. 18: Log-normal distribution functions extracted from the fit of the LZ relaxation curves of Fig. 17.

experiments. The resultant distribution functions for resonances  $k = 6, 7$  and  $8$  are shown in Fig. 18. The center of the distribution increases with the resonance number,  $k$ , while the width remains almost constant for different resonances, being somewhat narrower for resonance  $k = 8$ .

We have discussed in section IIb the two models that have been proposed to explain the presence of a broad distribution of tunnel splittings in terms of disorder. Before analyzing our results by using each model, note that a second order transverse anisotropy allows transitions for resonances  $2i$ , while fourth order anisotropy, which is imposed by the symmetry of the molecules, only allows MQT relaxation for resonance numbers multiple of 4,  $4i$ . Thus, a comparison between relaxation curves recorded at resonances  $k = 6$  and  $8$  should give us information about the origin of the tunnel splittings in this material. The relation between the tunnel splitting and the second order anisotropy is given by the next formula which follows from perturbation theory [35],

$$\ln(g_k) = \ln \left( \frac{E}{2D} \right); \quad (12)$$

where  $g_k$  and  $\Delta_k$  depend on  $k$ ,  $S$  and  $D$  [35] and were given in section IIa. Through this expression we can infer the distribution of second order anisotropy parameters,  $f(\ln(E/2D))$ , by taking the log-normal distributions used to fit the relaxation curves of resonances  $k = 6$  and  $k = 8$ . The results are shown in Fig. 19. The fact that both distributions do not scale when plotted as a function of  $\ln(E/2D)$  indicates that second order anisotropy can not be the only origin of tunnel splittings within the sample.

The distribution function of the second order anisotropy parameter predicted by the line dislocations model is given by [15],

$$f_L(x) = \frac{1}{2} \frac{1}{\sigma \sqrt{E_c}} \exp \left[ -x \frac{e^{2x}}{(2E_c)^2} \right]; \quad (13)$$

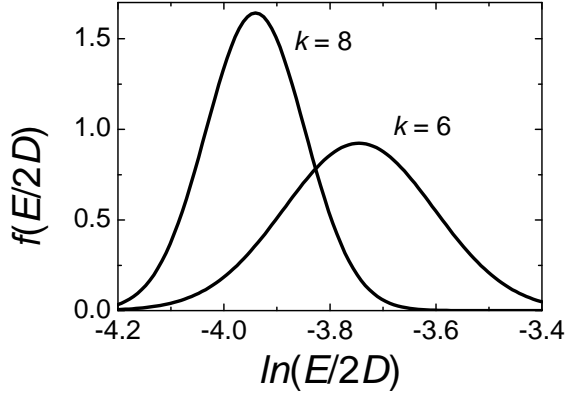


FIG. 19: Distribution of second order anisotropy parameter inferred from the log-normal distribution functions of resonances  $k = 6$  and  $8$  of Fig. 18 by using the expression of eq. (11).

where  $x = \ln E^*$  with  $E^* = E/2D$ .  $E_e^*$  is the width of the distribution of the anisotropy parameter  $E^*$ .  $E_e^*$  depends on the geometry of the crystal and on the concentration of dislocations per unit cell,  $c$ . Note that the mean value and width of the distribution given by this expression are not independent variables. By using this distribution with eq. (11) we have fitted the relaxation curve recorded at resonance  $k = 6$ . The only free parameter in the fit is  $E_e^*$ . The result is shown in Fig. 20 (thin line) where the log-normal distribution extracted from our previous fit of the same relaxation curve has been included for comparison (thick line). We have chosen the mean value to be at the same position as that of the log-normal distribution. The value of  $E_e^*$  used to fit the data corresponds to a concentration of dislocations per unit cell of  $c = 10^4$ . Clearly, the width of this distribution is many orders of magnitude bigger than the log-normal distribution used to fit our data. This is due to the fact that the distribution of  $E$  predicted from the line dislocations model has a most probable value at  $E = 0$ , which explains the long tail observed for low tunnel splitting values. Consequently, line dislocations would produce a much broader relaxation curve than that observed in the experiments. Our data indicates that a distribution of second order anisotropy with a non zero mode is needed to explain the MQT relaxation in Mn<sub>12</sub>-acetate.

We want to note that we were able to fit the relaxation curves by using a discrete multi-peak distribution of  $E$  values similar to that expected from the solvent disorder model [16]. However, it was necessary to include a gaussian width to each peak of the distribution in order to fit the data [17]. The values of the peak centers of this distribution for resonance  $k = 6$  are  $x_{c;1} = -7.19$  ( $-7.0525$ ),  $x_{c;2} = -8.55$  ( $-8.1749$ ), and  $x_{c;3} = -6.60$  ( $-6.7995$ ), (the values between parenthesis are extracted from ref. [16]). The width of each peak is  $W_i = x_{c;i}/50$  and the height of each peak was taken to be proportional to the population of the corresponding isomer given in ref. [16].

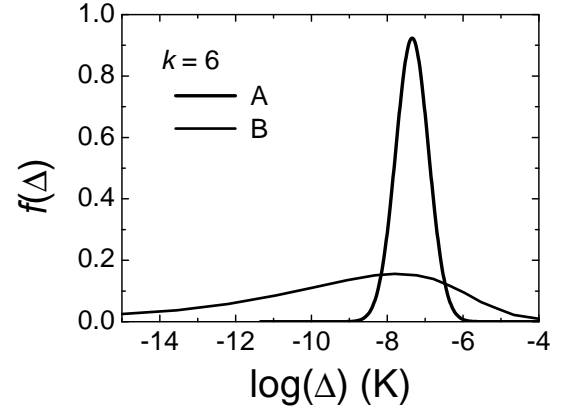


FIG. 20: Tunnel splitting distribution of resonance  $k = 6$  expected by line-dislocation model (thin line) compared with the log-normal distribution that fits the experimental data (thick line).

To conclude this subsection, we have shown that a multi-crossing LZ method allows the determination of the complete distribution of tunnel splittings for several resonances in SMMs. Our results suggest that a distribution of second order transverse anisotropies with a non zero mean value is necessary to explain the experimental data. The solvent disorder model provides such a source type and a discrete multi-peak distribution of tunnel splittings can be used to fit our data. However, some other type of disorder (i.e. line-dislocations or point defects) that introduces a small broadening of these peaks is also necessary to model the experimental data.

### C. MQT Symmetry Measurements

In this subsection we will present LZ relaxation experiments carried out in the pure quantum regime ( $T = 0.6$  K). In order to check the MQT symmetry imposed by the transverse terms of the Hamiltonian we have studied the LZ relaxation of the magnetization by sweeping an external longitudinal field,  $H_L$ , at a constant rate,  $\dot{H}$ , across a resonance  $k$  in the presence of an external transverse field,  $H_T$ , applied at arbitrary directions,  $\theta$ , with respect to the crystallographic axes of a Mn<sub>12</sub>-acetate single crystal. As we have shown in section II (i.e. see Fig. 4), MQT has an oscillatory response as a function of the orientation of a transverse field. This leads to maxima and minima in the MQT relaxation rates whose positions and symmetry depend on the transverse anisotropy term that generates the tunnel splittings. To recall, a fourth order anisotropy term would generate a fourfold rotation pattern in the MQT probability with maxima spaced by 45 degrees, while a twofold rotation pattern with spacing between maxima of 90 degrees is expected from a second order anisotropy term in the Hamiltonian. When two non-collinear different order transverse anisotropy terms are present, the symmetry of the MQT relaxation rates depends on the relative orientation between the anisotropy

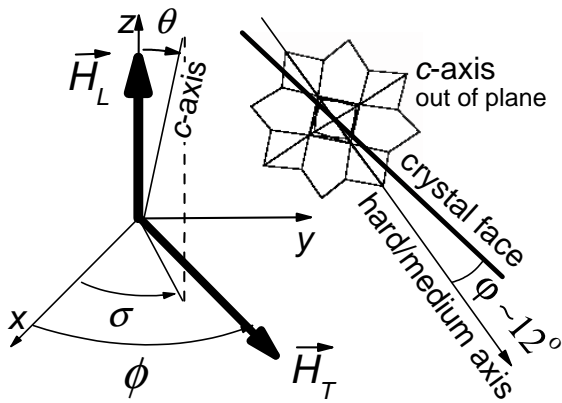


FIG. 21: Representation of the orientation of the c-axis (easy axis) of a crystal with respect to the axes of the applied external magnetic field ( $x, y, z$ ). The misalignment is determined by  $\theta$  and  $\sigma$ . The misalignment between the transverse magnetic axes of the  $M_{n_{1,2}}$ -acetate molecules and one of the faces of the crystal ( $\phi \sim 12^\circ$ ) is also shown.

axes.

A single crystal of  $M_{n_{1,2}}$ -acetate SMM was placed over a high sensitivity micro-Hall magnetometer as described at the first paragraph of this section. However, for these studies it is very important to know the exact orientation of the crystallographic axes with respect to the direction of the external magnetic field. Fig. 21 shows a sketch of the orientation of the c-axis of the crystal with respect to the external magnetic field. Note that in  $M_{n_{1,2}}$ -acetate the c-axis corresponds to the easy magnetic axis of the molecules. However, there is a misalignment of  $\phi \sim 12^\circ$  between the transverse magnetic axes (imposed by the fourth order anisotropy of the molecules) and the crystallographic axes. This is also shown in Fig. 21.

During the manual alignment of the crystal one of its faces was placed coplanar with the micro-Hall sensor plane with the help of a microscope. However, there exists an uncertainty of about  $\pm 5$  degrees in this orientation. This misalignment is represented by the angles  $\theta$  and  $\sigma$  in Fig. 21 and can be determined experimentally through magnetic measurements described below. The main implication of this misalignment is that there is a transverse field component due to the high longitudinal field applied along the z-axis that depends on the angles  $\theta$ ,  $\sigma$ , and  $\phi$ . The latter is the angle of application of the external transverse field with respect to the x-axis. Due to this, the total transverse field felt by the molecules in the presence of a constant transverse field,  $H_T$ , applied along  $y$  and with a longitudinal field,  $H_L = H_z \cos \theta$  ( $\cos \theta = 1$  for small  $\theta$ ) is given by,

$$H^2 = H_T^2 \cos^2(\theta) + H_L^2 \sin^2 \theta + H_T^2 \sin^2(\theta) \sin^2(\phi) \quad (14)$$

Thus, the transverse field felt by the molecules will have a minimum value for  $\phi = 0$  and a maximum for  $\phi = \pm 180^\circ$  with  $H_L > 0$ . The opposite situation would be found for  $H_L < 0$ . As we will show, once the misalignment angles are known, an algorithm can be used

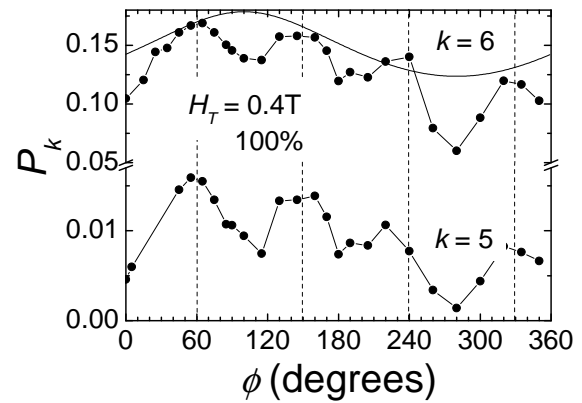


FIG. 22: MQT relaxation probability of resonances  $k = 6$  and  $7$  as a function of the angle  $\phi$ , of the applied transverse field,  $H_T = 0.4$  T, with respect to one of the faces of the crystal. The measurements were carried out starting from saturation (all the molecules within the crystal contributed to the relaxation).

to correct the applied fields in order to have a constant transverse field during the measurements, independent of the angle of application of the external fields.

In our first experiment we have studied the MQT relaxation rates of several resonances in the presence of a constant transverse field applied at arbitrary directions with respect to the crystallographic axes. The experiment was done as follows: We start with the initial magnetization of the sample equal to positive saturation,  $M_{\text{initial}} = +M_s$ , by applying a high longitudinal magnetic field,  $H_L = 6$  T. For this initial situation, all the molecules of the crystal were in the  $m = +10$  level in one of the energy wells. Then we turn on a transverse magnetic field,  $H_T = 0.4$  T, applied along a direction  $\phi$ , and sweep the longitudinal field at a constant rate,  $\dot{H} = 6.6 \times 10^3$  T/s. We measured the magnetization change in several resonances  $k$  and extracted the MQT probability by using  $P_{LZ} = (M_{\text{before}} - M_{\text{after}}) / (M_{\text{before}} - M_{\text{eq}})$ , where, in this case,  $M_{\text{eq}} = M_s$ . Note here that all the molecules within the crystal contribute to the relaxation. We repeated this procedure for different angles  $\phi$  from  $0$  to  $360$  degrees.

The behavior of the measured MQT probability as a function of  $\phi$  is shown in Fig. 22 for resonances  $k = 5$  and  $k = 6$ . The results clearly show a fourfold rotation pattern of MQT probability with maxima spaced by  $90$  degrees ( $\phi_{\text{max}} = 60^\circ; 150^\circ; 240^\circ$  and  $330^\circ$ ) for both resonances. Note that  $k = 5$  and  $6$  are the first observed resonances and  $\sim 35\%$  of the magnetization relaxes. This means that molecules that contribute to this relaxation are mainly those with among the biggest tunnel splitting values within the distribution.

There is also a onefold contribution that is represented by a continuous line in Fig. 22 with the result for resonance  $k = 6$  [43]. This oscillation is due to the misalignment of the c-axis of the crystal with respect to the applied magnetic field. This misalignment is represented by the angles  $\theta$  and  $\sigma$  and can be determined through

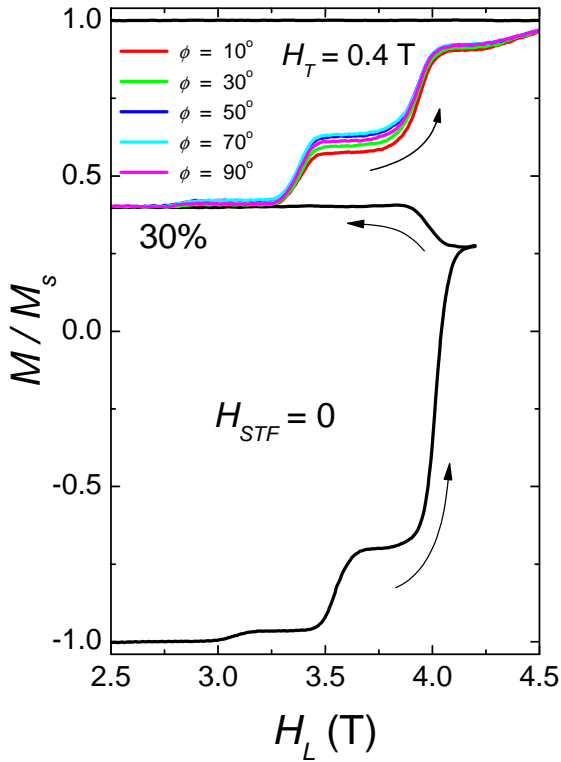


FIG. 23: (Color on-line) Selection of 30% of the molecules with the smallest tunnel splittings within the distribution. Starting at  $M = M_s$  the longitudinal magnetic field is swept from 0 to 4.2 T and back to 0 in the absence of a transverse field (black line). After that only those molecules that have not relaxed (30%) remain in the metastable well. Then a transverse field of 0.4 T is applied at an angle  $\phi$  and the longitudinal field is swept again to a high positive value. The process is repeated for different angles (lines with different colors).

magnetic measurements. From the results shown in Fig. 22 we can extract  $\phi = 80^\circ$  (where we observe the maximum value of the onefold contribution). To obtain  $\phi$ , we measured the behavior of the MQT probability of resonance  $k = 6$  for different magnitudes of the transverse field from  $-0.4$  to  $0.4$  T applied along  $\phi = 0^\circ$ . The transverse field value for which the probability is minimum (null real transverse field) gives the angle of misalignment through  $H_T (P_{\min}) = H_L \sin \phi$ , where  $H_L \sin \phi$  is the transverse projection of the longitudinal field. The value extracted for the misalignment is  $\phi = 0.3$ . The effect of this misalignment on the transverse field is larger the greater the resonance number. We do not show the results for higher resonances, such as  $k = 8$ , because the fourfold symmetry is almost unobservable due to the high onefold contribution of the misalignment.

In order to measure the response of the MQT probability versus angle  $\phi$  in other parts of the tunnel splitting distribution we have conducted LZ relaxation experiments in the following manner. We select a small fraction of molecules with the smallest tunnel splittings of the distribution, in contrast to the biggest values that were analyzed in the previous experiments. The measurement

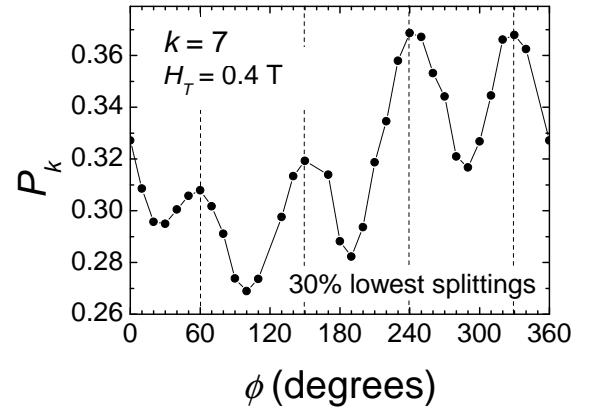


FIG. 24: MQT probability of resonance  $k = 7$  versus the angle,  $\phi$ , of the applied transverse field,  $H_T = 0.4$  T, with respect to one of the faces of the crystal. A previous selection process was used to study only 30% of the molecules with smallest splittings values within the distribution. The results were extracted from longitudinal magnetic field relaxation curves recorded at a constant rate,  $\dot{H} = 6.6 \cdot 10^3$  T/s.

method is presented in Fig. 23. We start with  $M = M_s$  by applying a high negative longitudinal magnetic field,  $H_L = -5$  T. Then we sweep the longitudinal field at a constant rate,  $\dot{H} = 6.6 \cdot 10^3$  T/s, up to  $H_L = +4.2$  T (just after crossing resonance  $k = 8$ ) and sweep it back to zero, crossing again resonances  $k = 8, 7, 6$ ... The whole selection process is done in the absence of a transverse field. After that, the net magnetization of the sample is  $M = 0.4M_s$ . This means that 70% of the molecules have relaxed to the stable well or, in other words, only 30% of the molecules have remained in the metastable well and will contribute to further relaxation. The latter are those molecules with the smallest tunnel splitting values within the distribution. After this, we turn on a transverse field,  $H_T = 0.4$  T, applied at an arbitrary angle,  $\phi$ , with respect to the crystallographic axes of the sample and we sweep the longitudinal field to a high positive value, crossing the resonances again. We repeated this procedure for different orientations of the transverse field from 0 to 360 degrees.

The MQT probability of resonance  $k = 6$  is shown as a function of  $\phi$  in Fig. 24. The results show the same fourfold symmetry pattern with maxima placed at the same positions than in the experiment shown in Fig. 22. As these two experiments study the relaxation of two different parts of the distribution of tunnel splittings (low and high ends of the distribution) we can conclude that the fourfold symmetry of MQT is a property of a significant fraction of the molecules within the crystal.

In principle, the fourfold rotation pattern is consistent with a fourth order transverse anisotropy term,  $C(S_+^4 + S_-^4)$ , in the spin-Hamiltonian (see Eq. 4b). For positive  $C$ , the four maxima generated by this term should be at  $\phi_{\max} = 45^\circ; 135^\circ; 225^\circ$  and  $315^\circ$ . There is a difference of 15 degrees between these values and those

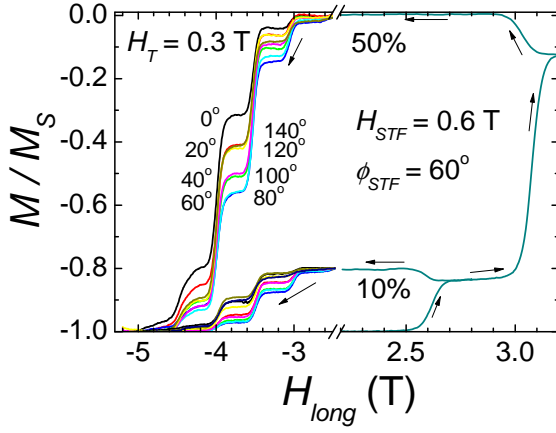


FIG. 25: (Color on-line) Selection processes carried out by sweeping a positive longitudinal field across resonances  $k = 5$  and  $6$  in the presence of a selection transverse field,  $H_{STF} = 0.6$  T, applied at a selection angle  $\phi_{STF} = 60^\circ$ . Both 10% and 50% of the molecules with the highest splitting values were selected in separate processes for further study with negative longitudinal field sweep in the presence of a transverse field,  $H_T = 0.3$  T, applied at different angles from  $0$  to  $360$  degrees.

observed in our experiments  $m_{ax} = 60; 150; 240$  and  $330$ . This is due to the misalignment,  $\delta = 12^\circ$ , between the hard anisotropy axis of the molecules and one of the faces of the crystal, which we use as the origin of our rotation. There still is a difference of  $3$  degrees that is within the accuracy with which we orient the crystal ( $\pm 5$  degrees). However, the value of  $C = 3 \cdot 10^5$  K cannot explain the difference between  $m_{ax}$  and  $m_{min}$  magnitudes of the measured MQT probability. The observed normalized changes,  $(P_{max} - P_{min})/P_{max}$ , in the experiment with the 100% of the molecules contributing to the relaxation are  $0.9$  for  $k = 5$  and  $0.6$  for  $k = 6$  (see Fig. 22). Whereas with this value of  $C$  we expect this change to be within the noise of the measurement.

In order to determine whether this symmetry is intrinsic to the  $Mn_{12}$  molecules and what is its origin, we have carried out experiments designed to select different parts of the distribution by using transverse fields in the selection process. Note that in the previous experiment we selected the smallest splittings of the sample in the absence of transverse fields. Now, we use a selection transverse field (STF),  $H_{STF}$ , applied at an angle,  $\phi_{STF}$ , during the preparation of the initial state of the system. In this case, those molecules with the medium anisotropy axis aligned with the STF have larger tunnel splitting values (larger relaxation probability) and can be selected for further study.

The measurements with this selection process are shown in Fig. 25. First we apply a high longitudinal field to saturate the magnetization of the system and sweep the field back to zero, having at the end a magnetization,  $M = M_S$ . Then we turn on a selection transverse field,  $H_{STF} = 0.6$  T, applied at the angle  $\phi_{STF} = 60^\circ$  where one of the four maxima were observed in the experiments

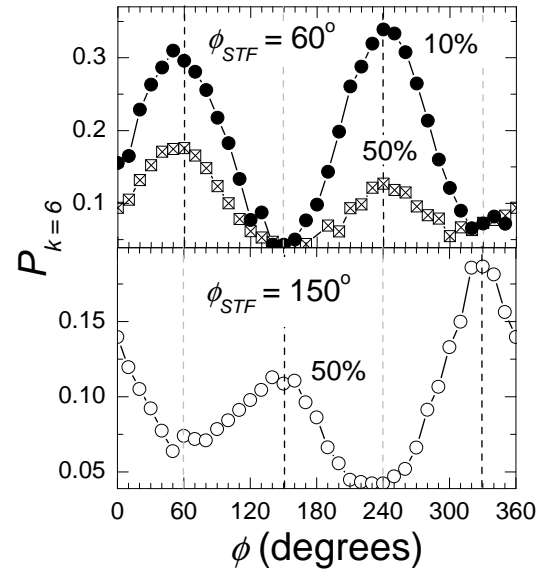


FIG. 26: Behavior of the MQT probability versus the angle of application of a transverse field,  $H_T = 0.3$  T, with previous selections of a part of the tunnel splitting distribution by using a selection transverse field,  $H_{STF}$ , applied along the directions where two complementary maxima were observed in the experiments with the whole sample,  $\phi_{STF} = 60^\circ$  (upper figure, for both 10% and 50% of the biggest splittings of the distribution) and  $\phi_{STF} = 150^\circ$  (lower figure, for 50% of the biggest splittings).

carried out with the whole sample, and we sweep the longitudinal field at a constant rate to a positive value and sweep back to zero. The value of this field is chosen depending in how much relaxation we want in the selection process: For the selection of 50% of the biggest splittings we sweep the field up to  $3.2$  T allowing the system to relax in resonances  $k = 5$  and  $6$ , for the selection of the 10% of the biggest splittings we only allow the system to relax in resonance  $k = 5$ . The final states of the magnetization are  $M = 0$  and  $M = 0.8M_S$  respectively. After the selection process we sweep the longitudinal field down to  $-5.5$  T at a constant rate,  $\dot{H} = 6.6 \cdot 10^3$ , in the presence of a transverse field,  $H_T = 0.3$  T, applied at different angles with respect to one of the faces of the crystal. We repeated this procedure for different angles from  $0$  to  $360$  degrees. In a separate experiment, we repeated the selection of 50% of the molecules with highest splittings within the distribution by applying a selection transverse field,  $H_{STF}$ , along the angle in which a complementary maximum was observed,  $\phi_{STF} = 150^\circ$ .

The results are shown in Fig. 26. It is clearly observed in all the selections that the MQT probability shows a twofold rotation pattern with maxima spaced by  $180$  degrees. For the selection in which  $H_{STF}$  is applied along  $\phi_{STF} = 60^\circ$ , the two maxima are at  $m_{ax,1} = 60^\circ$  and  $m_{ax,2} = 240^\circ$ , for both fractions of molecules selected (10% and 50%). Moreover, when the selection field is applied along the position of a complementary fourfold maximum,  $\phi_{STF} = 150^\circ$ , the twofold maximum,

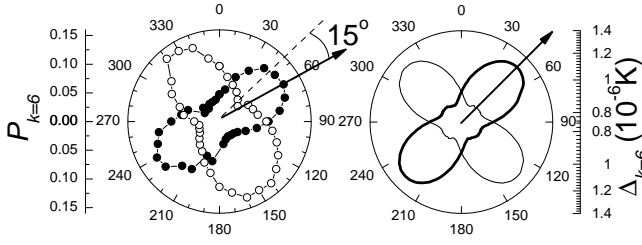


FIG. 27: Left: Experimental observations of the MQT probability of resonance  $k = 6$  for complementary directions of the transverse selection field. The onefold contribution coming from the misalignment and has been corrected for clarity. Right: Calculated tunnel splitting of resonance  $k = 6$ ,  $\theta_{k=6}$ , for  $\phi = 30^\circ$  and opposite signs of  $E$ , by using the same values of  $H_{TF}$ ,  $D$ ,  $E$  and  $C$  used in Fig. 9.

$\theta_{max;1} = 150^\circ$  and  $\theta_{max;2} = 330^\circ$ , are displaced by 90 degrees with respect to the previous case.

The observation of twofold rotation pattern in MQT probability is a clear evidence of a second order transverse anisotropy lower than that imposed by the site symmetry of the molecule (fourth order). This is in excellent agreement with the solvent disorder model proposed by Comia et al. [16] where there is an expectation of equal populations of molecules with opposite signs of the second order anisotropy. A considerable increase of the change of probability between maxima and minima is also observed as the fraction of molecules with highest tunnel splitting values becomes smaller, indicating the fact that the molecules with largest splitting values have bigger values of the second order anisotropy.

In section II we stated that two non-collinear anisotropy terms would considerably modify the magnetic response of the molecules to the orientation of a transverse magnetic field depending on the angle of misalignment,  $\theta$ , between both anisotropies (see eqs. (5) and (6) and Fig. 5). The symmetry of MQT probability expected from this model depends on several parameters like the resonance number,  $k$ , and/or the misalignment angle,  $\theta$ , between non-collinear anisotropies. It turns out from this model that for  $\theta_{j < 30} \text{ mK}$  (bigger than the maximum  $E$  value expected from the solvent disorder model) the symmetry of the MQT probability mainly depends on the angle of misalignment,  $\theta$ , going from fourfold for small values to twofold for big values. Taking a given  $E$  value, the transition between fourfold to twofold maxima patterns as a function of  $\theta$  depends on the resonance number  $k$  we are considering. For example, for resonance  $k = 0$  (Fig. 8A), the fourfold maxima pattern is observed for every misalignment value, where a slight twofold modulation is due to the second order anisotropy. For bigger resonances (i.e.  $k = 6$ ), the transition between these two MQT probability symmetries is cleaner (see Fig. 9). For misalignment angles,  $\theta_{j < 20}$ , MQT probability shows fourfold symmetry modulated by the second order anisotropy. However, for angles  $\theta_{j > 20}$  the MQT probability symme-

try is twofold. Consequently, the observation of twofold symmetry in our experiments shows that the angle of misalignment between both anisotropy orders is greater than 20 degrees. In section IV we will present high frequency EPR experiments that show that the angle of this misalignment is  $\theta = 30^\circ$ . In Fig. 27 we show a comparison between the experimental observation of resonance  $k = 6$  for both transverse selection fields with 50% of the biggest splittings (left polar plot) and the calculated splitting (right polar plot) corresponding to resonance  $k = 6$  and  $\theta = 30^\circ$  with opposite signs of  $\theta_{j = 30} \text{ mK}$ . The difference of 15 degrees between the experimental results and the calculations is also shown in this figure. As we said before, this difference is due to the fact that we measure the angle  $\theta$  with respect to one of the faces of the crystal while the transverse magnetic axes of the molecules are rotated from the faces of the crystal by 12 degrees.

An estimation of the values of  $E$  needed to explain the experimental observations of the oscillation of the MQT probability presented in this subsection are: a)  $E = 0.5 \text{ mK}$  for the result corresponding to the 30% of the smallest splittings of the distribution (Fig. 24), b)  $E = 2.5 \text{ mK}$  for the result with the whole distribution (Fig. 22, upper curve) and with 50% of the biggest splitting in the selection with  $H_{STF} = 60$  and 50 (Fig. 26), and c)  $E = 10 \text{ mK}$  for the result corresponding to 10% of the biggest splittings of the distribution (Fig. 26, solid circles). These values are in excellent agreement with the results obtained by high frequency EPR experiments (that will be shown in section IV) and by recent density functional theory calculations [45]. However, they are slightly larger than the values initially proposed in ref. [16].

#### D. Berry Phase Measurements

The ability to select a subset of molecules with a narrow distribution of tunnel splittings and, for example, different signs of the second order transverse anisotropy allows us to study the behavior of the MQT relaxation as a function of a transverse field. As we anticipated in section II, quantum phase interference (Berry phase) would lead to zeros of the tunnel splittings (i.e. absence of magnetic relaxation) for several values of a transverse field applied along the hard anisotropy axis of the molecules and we discussed how the pattern of the oscillations can be modified by the presence of two non-collinear transverse anisotropies.

For these experiments we have used the same preparations of the initial states of the system than those shown in Fig. 25. This initial states of the system correspond to a selection of 50% and 10% of the molecules of the sample with higher values within the tunnel splitting distribution. The selection of both initial states is done by applying a selection transverse field,  $H_{STF} = 0.6 \text{ T}$ , at an angle  $\theta_{STF} = 60^\circ$ . As we have shown this proce-

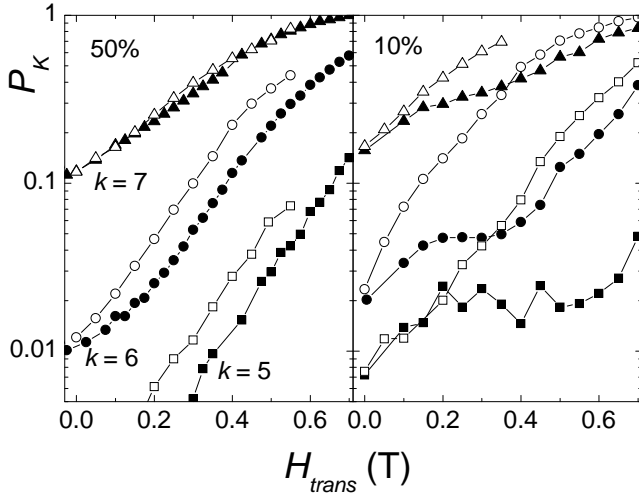


FIG. 28: MQT probability of resonances  $k = 5, 6$  and  $7$  as a function of the magnitude of a transverse field applied along  $\alpha = 60$  (open symbols) and  $\alpha = 150$  (solid symbols). The initial state of the sample was prepared by selection of 50% (left) and 10% (right) of the molecules with biggest tunnel splitting values by using a selection transverse field,  $H_{STF} = 0.6$  T, applied along  $\alpha_{STF} = 60$ . The two directions of variation of the transverse field correspond to where the first maximum ( $\alpha = 60$ ) and minimum ( $\alpha = 150$ ) of the twofold rotation pattern were observed.

ture mainly selects those molecules with one E-sign as is observed in the twofold transverse field rotation pattern of the MQT probability of Fig. 26, with maxima at  $\alpha_{max} = 60; 240$  and minima at  $\alpha_{min} = 150; 330$ . To study the behavior of the MQT probability as a function of the magnitude of the applied transverse field we apply a transverse field,  $H_T$ , along the direction of the first maximum,  $\alpha = 60$ , after the selection process and we sweep the longitudinal field at a constant rate to  $\sim 5.5$  T, measuring the change of magnetization in each resonance crossing. We do the same procedure for different values of the transverse field from  $H_T = 0$  to  $0.7$  T. Moreover, we repeated the same measurement by applying the transverse field along the direction of the first minimum  $\alpha = 150$  [44]. The results of MQT probability for resonances  $k = 5, 6$  and  $7$  are shown in Fig. 28. In the left graph of the figure are the results obtained with 50% of the molecules with highest splitting values. In the right graph we show the results for 10% of the biggest splittings. The measurements with the transverse field applied along the first of the twofold maximum,  $\alpha = 60$ , are represented by open symbols, while the solid symbols correspond to measurements with the transverse field applied along the first of the minimum,  $\alpha = 150$ .

There are several important aspects to this figure. a) There is vertical shift between the curves corresponding to different directions of application of the transverse field. The shift is bigger in the case of the selection of the 10% of the biggest splittings within the distribution. This is consistent with the observations of Fig. 26 and

supports the assumption of a distribution in the magnitude of the second order anisotropy. b) MQT probability increases exponentially with the magnitude of the transverse field. This is expected from the exponential dependence of the LZ probability on the tunnel splitting shown in eq. (8), and the power law dependence of the tunnel splitting on the magnitude of the transverse field (see eq. (3)) [35]. There are significant deviations from the exponential behavior in the right hand graphic for a transverse field applied along the first of the twofold minimum,  $\alpha = 150$ . The largest deviations are observed at fields  $H_p(k = 5) = 0.45$  T,  $H_p(k = 6) = 0.3$  T and  $H_p(k = 7) = 0.35$  T. This is reminiscent to the Berry phase observed in  $Fe_3$  [33].

The results shown on the right graph of Fig. 28 can be compared to the calculations of the tunnel splitting versus the transverse field shown in Fig. 13 that were done taking into account two non-collinear anisotropy terms in the Hamiltonian (eqs. (5) and (6)). In fact, the values,  $E = 10$ – $15$  mK, used in these calculations were chosen according to the results shown in Fig. 28 and agree with the values extracted from high frequency EPR measurements (section IV). The agreement between theory and experiments is very good and constitutes the first evidence of quantum interference phenomena in a SMM system with two non-collinear transverse anisotropies of different order. Note that none of the directions of application of the transverse field in these studies correspond to any of the hard axes of the anisotropy terms separately.

#### E. Summary of magnetic relaxation experiments

We have shown in this section that LZ magnetic relaxation experiments allow us to determine the complete distribution of tunnel splittings of  $Mn_{12}$ -acetate. The results obtained through a multi-crossing LZ method show that a distribution of second order anisotropies with non-zero mode is required in order to explain our data, such as in the solvent disorder model proposed by Comia et al. [16]. LZ relaxation experiments carried out in the presence of a transverse field applied at arbitrary directions with respect to the crystallographic axes of the sample enabled studies of the symmetry of the MQT probability. We have shown that MQT probability has a general fourfold rotation pattern as a function of the orientation of a transverse field. This is associated with equal population of molecules with opposite signs of a second order transverse anisotropy. The LZ method allows the selection of a subset of molecules with different values of the tunnel splitting for further study. By the application of a transverse field in the selection process we are able to select a fraction of molecules of the sample with lower anisotropy order and different signs of E. Using this selection procedure we have studied a small fraction of molecules with one sign of E and the largest tunnel splitting values within the distribution. These show an unusual Berry phase phenomena for several transverse field

values that does not lead to complete zeroes in the tunnel splitting. Our results on the symmetry of MQT magnetic relaxation can be explained in terms of two non-collinear different order transverse anisotropies in the Hamiltonian that explain, among other things, why the observed Berry phase phenomena does not depend in any simple way on that expected from either anisotropy term alone.

#### IV. HIGH FREQUENCY EPR EXPERIMENTS

High frequency (40 to 200 GHz) single crystal Electron Paramagnetic Resonance (EPR) measurements were carried out using a millimeter-wave vector network analyzer (MVNA) and a high sensitivity cavity perturbation technique; this instrumentation is described elsewhere [46]. Temperature control in the range from 2 K to room temperature was achieved using a variable-flow cryostat. The magnetic field was provided by a horizontal superconducting split-pair magnet with vertical access, enabling angle dependent studies (< 0.1° resolution) and approximate alignment of the single crystal [27]. In order to make accurate comparisons with the magnetization studies presented in the preceding sections, all data presented in this section were performed on a single deuterated crystal of  $Mn_{12}$ -acetate ( $d-Mn_{12}$ -ac), having approximate dimensions  $1.0 \times 3.0 \times 3.0$  mm<sup>3</sup>. This crystal was selected from a batch of samples which had previously been removed from the mother liquor and stored for 1 year in a refrigerator (at 5° Celsius) prior to the measurement. This particular batch was grown using standard methods [41], albeit in a completely independent synthesis from the samples used for the magnetization measurements. The sample was separately cooled under vacuum from room temperature at 5 K/minute in one of two orientations for field rotation in i) the  $x-y$  plane, and ii) a plane perpendicular to the  $x-y$  plane. In the former case, the sample was mounted on the side wall of a cylindrical TE<sub>011</sub> cavity (center frequency = 53.1 GHz,  $Q = 20,000$ ) with its easy axis parallel to the cavity axis such that the microwave field  $H_1$  was aligned parallel to the sample's easy axis (and, therefore, perpendicular to the applied DC field). In the latter case, the sample was mounted on the end plate of the same cavity, and DC field rotation was carried out for angles close to the  $x-y$  plane (within 15°), with the microwave  $H_1$  field again parallel to the sample's easy  $z$ -axis. Field sweeps were restricted to 6.6 T due to limitations of the split-pair magnet. As will become apparent, the data obtained for the  $d-Mn_{12}$ -ac are in qualitative agreement with earlier published results obtained for the hydrogenated  $Mn_{12}$ -ac [19, 27].

#### A. Magnetic symmetry measurements in the high-field limit

In the preceding sections, it has been shown how the Landau-Zener method may be applied to SMMs in order to determine very weak transverse terms in Eq. (1). Moreover, the Landau-Zener method allows one to select molecules, based on the tunneling rates of the different species. Subsequently, by performing angle dependent studies on each sub-species, one can deduce the underlying symmetries of the dominant tunneling matrix elements. While this method is extremely powerful, it is evident from the discussion in section II.C that, for systems with multiple sources of transverse anisotropy (intrinsic and extrinsic), deconvolution of the different contributions to the tunnel splittings can be problematic, i.e. in Figs. 6 to 9 it is seen that competing E and C terms results in a competition between the two-fold and four-fold symmetries of these interactions. The reason for this competition is that, at low-elds, the E and C terms operate in different high orders of perturbation theory, thereby resulting in a complicated interaction between the two perturbations.

At first sight, it is not obvious how EPR experiments, conducted in the GHz frequency range, could shed new light on the nature of transverse interactions which manifest themselves as miniscule tunnel splittings of order  $10^4$  Hz at low-elds. However, the so-called "tunnel splittings" are measured by the Landau-Zener method at low-elds wherein the transverse terms operate in very high orders of perturbation theory within an  $m_z$  basis (see Eq. (3)), where the quantization axis is defined by the global easy-axis of the crystal. For high magnetic fields applied in the transverse direction, such a picture is no longer valid due to the conflicting symmetries imposed by the crystal field and the applied field. Herein lies the beauty of the high-eld EPR technique. By applying a sufficiently strong transverse field, one can reach a limit in which the appropriate basis of spin states is defined by a quantization axis parallel to the applied field, i.e. the  $x$ -direction. In such a limit, transverse zero-eld interactions operate in zeroth-order. Consequently, their effects may be rather strong. As an illustration of this point, consider the simplest zero-eld Hamiltonian:

$$H = D S_z^2 + E (S_x^2 - S_y^2) + g_B H_x S_x; \quad (15)$$

Making a substitution for  $S_z^2$  in terms of  $(S_x^2 + S_y^2)$ , one obtains:

$$H = \frac{1}{2} (D + 3E) S_x^2 + \frac{1}{2} (D - E) (S_y^2 - S_z^2) + g_B H_x S_x; \quad (16)$$

which can be re-written as:

$$H = \frac{1}{2} (D + 3E) S_x^2 + g_B H_x S_x + H_T^0; \quad (17)$$

This equation is diagonal in  $S_x$ , and has the same form as Eq. (15). Therefore, to lowest order, the high-eld

eigenvalues will be given by:

$$(m_x) \quad \frac{1}{2} (D + 3E) m_x^2 - g_B H_x m_x ; \quad (18)$$

Similar arguments hold for higher order transverse terms. Thus, the transverse high-field EPR spectra provide perhaps the most direct means of measuring these transverse terms. Indeed, this represents one of the more illustrative examples of the importance of high-field EPR as a spectroscopic tool for studying quantum magnetism. Not only does the effect of the zero-field transverse terms shift to zeroth order, but the symmetry of such interactions is also preserved. This is best illustrated using the same example as above, with the field applied along the y-axis instead of the x-axis. In this case, Eq. (15) may be re-written:

$$H = \frac{1}{2} (D - 3E) S_y^2 - g_B H_y S_y + H_T^{00} ; \quad (19)$$

giving

$$(m_y) \quad \frac{1}{2} (D - 3E) m_y^2 - g_B H_y m_y ; \quad (20)$$

Thus, from Eqs. (18) and (20), it is apparent that the influence of the ( $E$ ) term changes sign upon rotating the applied field from the x-axis of the E-tensor to the y-axis. This two-fold behavior is not unexpected; indeed, it is obtained also from the exact diagonalization calculations shown in Figs. 6 to 8, which correspond to the high-field/frequency limit discussed here. However, unlike lower-field calculations, the 2<sup>nd</sup> and 4<sup>th</sup> order interactions decouple completely at high-fields, as do other transverse interactions. Thus, one may consider their effects completely independently. This point is illustrated in Fig. 8, where it can be seen that the effect of an intrinsic fourth-order anisotropy is to produce a ground-to-first-excited-state splitting ( $k=0$ ) which oscillates as a function of the field orientation within the hard/medium plane, with a periodicity of 90°. The disorder-induced rhombic anisotropy, meanwhile, has no effect on this four-fold behavior. Instead, it causes a two-fold modulation of the line width/shape. What is more, because of the complete independence of these effects, one can in principle determine any misalignment,  $\theta$ , between the hard axes associated with the second and fourth order transverse anisotropies, as illustrated in Fig. 8.

In order to make direct comparisons with other spectroscopic studies (e.g. neutron [12] and EPR [7, 13, 16]) we re-write the Hamiltonian of Eq. (1) in the following form:

$$\hat{H} = D [\hat{S}_z^2 - \frac{1}{2} \hat{S}(\hat{S}+1)] + E (\hat{S}_x^2 - \hat{S}_y^2) + B_4^0 \hat{O}_4^0 + B_4^4 \hat{O}_4^4 + \hat{H}_z \quad (21)$$

where  $\hat{H}_z = -g_B \hat{S}_z$  is the Zeeman term due to the applied magnetic field and  $\hat{O}_B^A$  are the Stevens' operators, of order  $B$  in the spin operators and possess  $A$ -fold symmetry (i.e.  $\hat{O}_4^4 = \frac{1}{2} (\hat{S}_+^4 + \hat{S}_-^4)$ ).

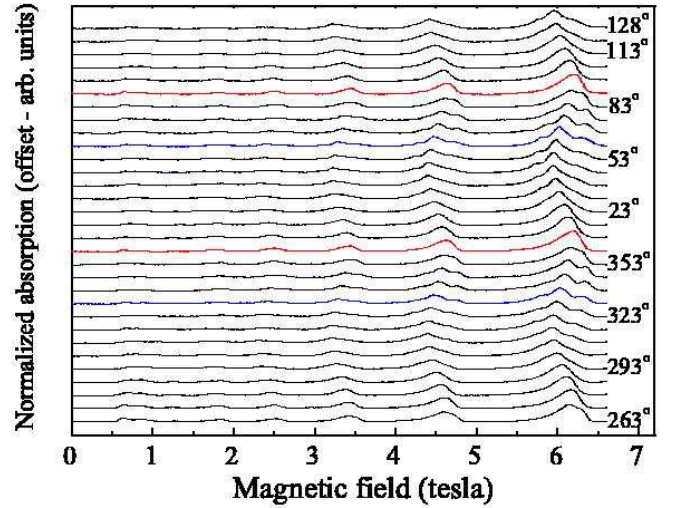


FIG. 29: (Color on-line) Microwave absorption obtained for different field orientations within the hard ( $xy$ -) plane of the sample; the temperature was 15 K and the frequency was 51.3 GHz in every case. The peaks in absorption correspond to EPR. The data were obtained at 7.5° intervals, where the angle refers to the field orientation relative to one of the  $\hat{a}$  edges of the square cross section of the sample. The resonances have been labelled according to the scheme described in ref. [27]. The blue traces correspond to field orientations approximately parallel to the hard/medium axes of the E-tensor, i.e. orientations corresponding to the maximum splitting of the low and high field shoulders. The red traces correspond to orientations of the hard axes of the  $B_4^0$  tensor.

Fig. 29 displays the raw microwave absorption obtained for different field orientations within the hard ( $x-y$ ) plane of the sample; the temperature was 15 K and the frequency was 51.3 GHz in every case. The peaks in absorption correspond to EPR. The data were obtained at 7.5° intervals, where the angle refers to the field orientation relative to one of the  $\hat{a}$  edges of the square cross section of the sample. The resonances have been labelled according to the scheme described in ref. [27]. For fields applied approximately parallel to the hard plane, only resonances are observed (resonances appear for field rotation away from the hard plane, see below). The highest field peak, 8, corresponds to an excitation between levels which evolve from the zero-field  $m_z = 9$  zero-field doublet. The transition from the ground state,  $m_z = 10$  ( $k=0$  resonance), is not observed within the available field range for these experiments; at 51 GHz, its expected position is at  $H_T \approx 9$  T. For a detailed discussion of the resonance labelling scheme, as well as the temperature, frequency, field and field orientation dependence of the EPR spectra for  $Mn_{12}$ -ac, refer to [27].

Immediately apparent from the Fig. 29 is a four-fold variation in the positions of each cluster of resonances (8, 6, etc.). Note that each of the resonances exhibit fine structures, which also depend on the field orientation; these are related to the disorder in the crystal, and we discuss this further below. The four-fold

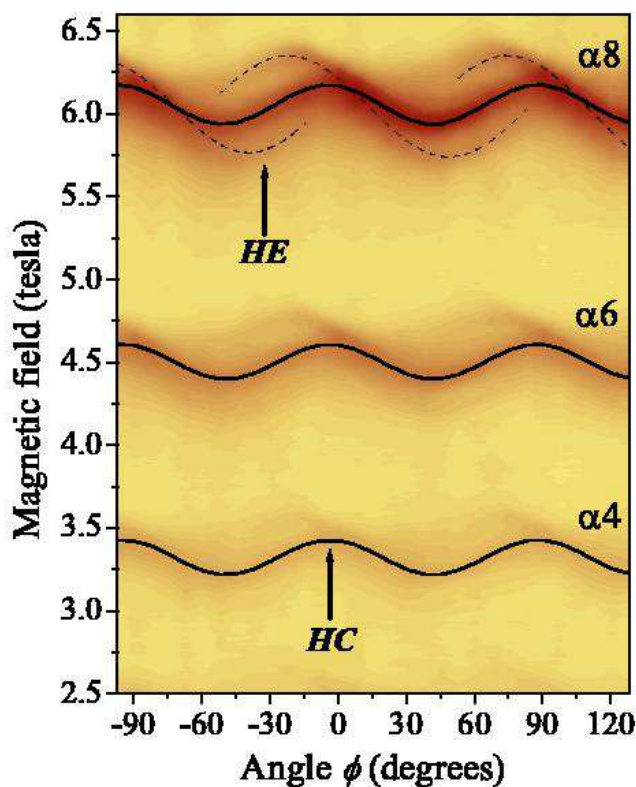


FIG. 30: (Color on-line) Color contour plot of the absorption intensity (see Fig. 29) versus magnetic field strength and the azimuthal angle  $\phi$ ; the darker shades correspond to stronger absorption. Superimposed on the absorption maxima are fits to the  $\phi$ -dependence of the central positions of each peak (solid lines). These fits assume accepted values for the zero-field parameters  $D$  and  $B_4^0$ , and a single value of the fourth-order transverse parameter  $B_4^4 = 3.2 \cdot 10^5 \text{ cm}^{-1}$ . Also superimposed on the  $\alpha 8$  absorption maxima are fits to the angle dependence of the high- and low-field shoulders (dashed curves). The approximate orientations of the hard axes corresponding to the  $E$  (HE) and  $B_4^4$  (HC) tensors are indicated.

shifts are due to the intrinsic fourth-order transverse anisotropy  $B_4^4 \hat{O}_4^4$ , as has previously been established for h-M  $n_{12}$ -ac [47]. Fig. 30 shows a color contour plot of the absorption intensity versus magnetic field strength and the azimuthal angle  $\phi$ . Superimposed on the absorption maxima are fits to the  $\phi$ -dependence of the central positions of each peak. These fits assume accepted values for the zero-field parameters  $D$  and  $B_4^0$  ( $D = 0.455 \text{ cm}^{-1}$  and  $B_4^0 = 2 \cdot 10^5$ ), and a single value of the fourth-order transverse parameter  $B_4^4 = 3.2 \cdot 10^5 \text{ cm}^{-1}$ . This is the only unknown parameter in the fit ( $D$  and  $B_4^0$  were verified independently from easy axis measurements), and all peak positions are consistent with a single value of  $B_4^4$ . We note that this value is in precise agreement with that found for h-M  $n_{12}$ -ac, as is to be expected for this fourth-order interaction which is related to the intrinsic symmetry of the  $M n_{12} O_{12}$  molecule. From the maxima and minima in the peak

position shifts induced by the  $B_4^4 \hat{O}_4^4$  term, we estimate that the hard and medium directions of this intrinsic crystal field interaction are oriented at  $\theta_{HC} = 45.5^\circ$  ( $+i90^\circ$ ) and  $\theta_{MC} = 41.5^\circ$  ( $+i90^\circ$ ) relative to the square edges of a typical single crystal sample.

Next we turn to the angle-dependent line structures which are very apparent in the ranges  $\phi = 300^\circ - 330^\circ$  and  $\phi = 30^\circ - 60^\circ$  in Fig. 29. The first point to note is the fact that we see shoulders on both the high and low-field sides of the main peaks in these angle ranges. This contrasts the situation found for h-M  $n_{12}$ -ac, where only high-field shoulders are observed. Furthermore, the high-field shoulder is far more clearly resolved in the present experiments on d-M  $n_{12}$ -ac. It has already been well established [19] that the shoulders may be understood within the context of the Comia solvent-disorder picture [16], wherein roughly 50% of the molecules have lower than four-fold symmetry due to a disorder effect associated with the acetic acid of crystallization. Remarkably, the present findings suggest that this disorder effect is more pronounced in the d-M  $n_{12}$ -ac than the h-M  $n_{12}$ -ac. The reason for the absence of a low-field shoulder in h-M  $n_{12}$ -ac has been ascribed to disorder-induced tilts of the molecules which are correlated with the disorder-induced rhombic anisotropy responsible for the splitting of the shoulders away from the main peaks [27]. The combination of these interactions results in a broader and, therefore, weaker low-field shoulder which is not resolved from the main peak in h-M  $n_{12}$ -ac. While both shoulders are clearly resolved in the present investigation, we see from Fig. 29 that the low-field shoulder is clearly weaker, and noticeably broader.

In order to make quantitative comparisons between the disorder effects in h-M  $n_{12}$ -ac and d-M  $n_{12}$ -ac, Fig. 30 shows the  $\phi$ -dependence of the splitting of the high and low-field shoulders for each of the main peaks ( $\alpha 8$ ,  $\alpha 6$ , etc.). This figure may be directly compared with Fig. 2 of ref. [27], which displays exactly the same data for the h-M  $n_{12}$ -ac complex. As discussed in ref. [27] and section III C of this article, the amplitude of the line width modulation (i.e. the extent of the splitting) is a measure of the disorder-induced rhombic anisotropy for the  $n = 1$  and  $n = 3$  variants in Comia's model. The splitting in the present study for d-M  $n_{12}$ -ac is roughly a factor of two greater than for the h-M  $n_{12}$ -ac, implying a factor of two increase in the  $E$  ( $0.02 \text{ cm}^{-1}$ ) value for the  $M n_{12}$  variants responsible for the shoulders. The possible origin of this unexpected result is discussed further below. Most importantly, this difference accounts for one of the few remaining inconsistencies between the magnetic measurements in ref. [18] and the EPR studies of ref. [27], which were carried out on d-M  $n_{12}$ -ac and h-M  $n_{12}$ -ac respectively.

The final point to note from the hard-plane rotation data is the phase shift between the four-fold modulation of the line position and the line shape. Indeed, this is one

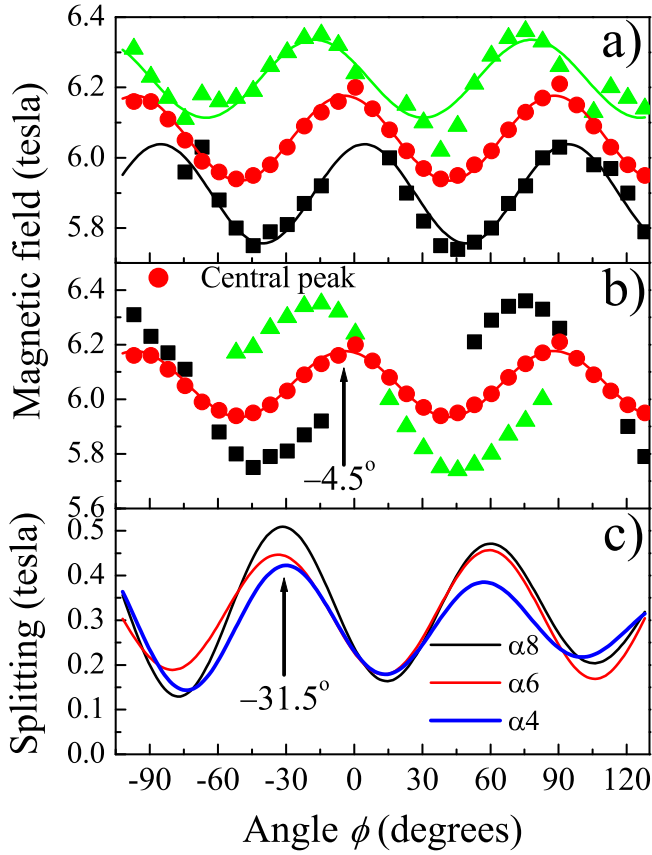


FIG. 31: (Color on-line) a) Hard-plane angle ( $\phi$ ) dependence of the splitting of the high and low-field shoulders, for the 8 peak. This figure may be compared with Fig. 2 of ref. [13], which displays similar data for the h-M  $n_{12}$ -ac complex. In (a), the positions of the low- (black) and high- (green) shoulders on 8 have been separately fitted with sine functions. The difference between these fits is displayed in (c), together with similar curves generated by the same procedure for peaks 6 and 4. The splittings plotted in (c) are a measure of the shifts caused by the disorder-induced rhombic term for the low-symmetry Comia variants [16] (see also Fig. 8); all curves are in agreement (within error) as to the orientation of the hard/medium two-fold directions. In (b), the data in (a) are plotted in such a fashion as to illustrate the real two-fold nature of the angle dependence of the high- and low- field shoulders. The approximate orientation ( $\phi = 4.5^\circ$ ) of one of the hard four-fold axes (HC) is indicated in (b), and the approximate orientation ( $\phi = 31.5^\circ$ ) of one of the hard/medium two-fold axes (HE) is indicated in (c).

of the main points of this article. As discussed in section II.C, this difference indicates a  $27 \pm 3$  misalignment of the  $\hat{O}_2^2$  and  $\hat{O}_4^4$  tensors, as was originally suspected for the h-M  $n_{12}$ -ac [18, 19]. The present study provides further support for this finding, thereby illustrating the remarkable differences between the global and local symmetries of M  $n_{12}$ -ac.

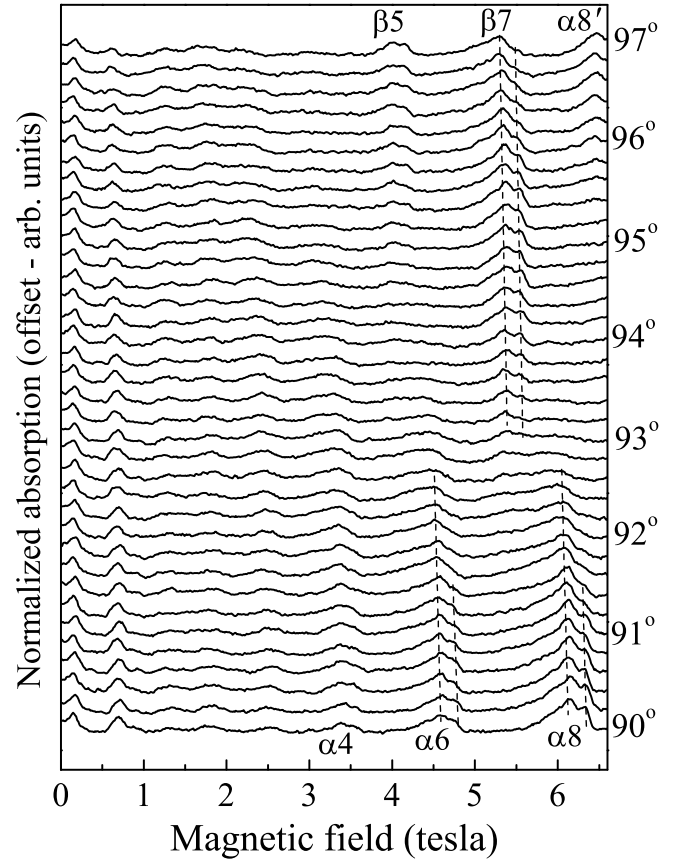


FIG. 32: (Color on-line) Microwave absorption spectra obtained at  $0.2^\circ$  intervals over the range from  $\phi = 90$  to  $97^\circ$  ( $\phi = 5^\circ$ ); the temperature was 15 K and the frequency was 51.3 GHz in every case, and the traces are offset for clarity. The peaks in absorption correspond to EPR, and the labelling is discussed in ref. [27]. See main text for discussion of the data.

## B. Easy-axis tilting

In this section, we briefly present the results of measurements for field rotations away from the hard plane in order to illustrate the presence of a small distribution of tilts of the easy axes of the d-M  $n_{12}$ -ac molecules. In the following figures, the polar angle  $\theta$  represents the angle between the applied DC magnetic field and the global easy axis of the crystal, i.e.  $\theta = 90^\circ$  indicates the hard/medium-plane direction. Field rotation was performed in a plane approximately parallel to one of the large flat surfaces of the needle-shaped crystal (i.e.  $\phi = 0^\circ$ , or  $90^\circ$ , etc.). A more extensive discussion of the analysis and interpretation of the results of similar experiments for the h-M  $n_{12}$ -ac complex have been published elsewhere [27]. Consequently, we present only data for d-M  $n_{12}$ -ac in this article, and discuss the implications without including detailed simulations, which will be published elsewhere [48].

Fig. 32 shows a series of absorption spectra obtained at

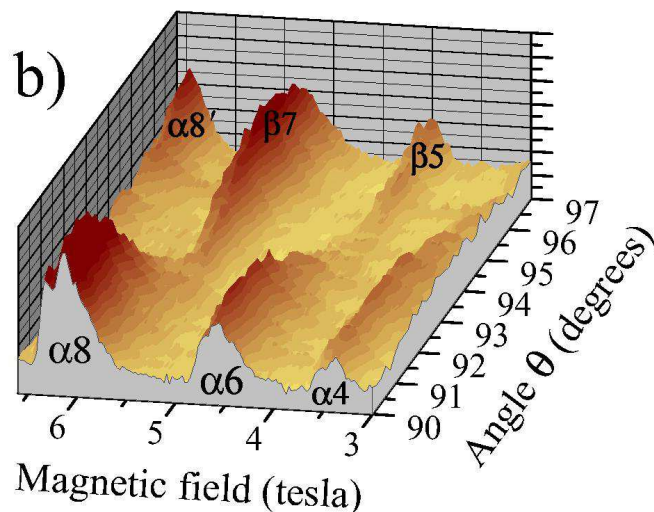
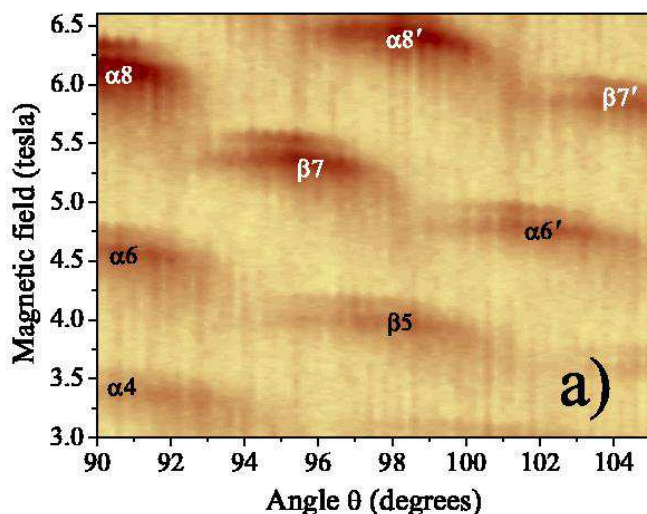


FIG. 33: (Color on-line) (a) A color contour map and (b) a 3D color surface plot representing the same data shown in Fig. 32 (the darker colored regions correspond to stronger EPR absorption). We plot the data in this manner for direct comparison with simulations shown in Fig. 6. The significant overlap of the  $\alpha$  and  $\beta$  resonances suggests tilting of the molecules. See main text and ref. [27] for discussion.

0.2 intervals over the range from  $\theta = 90$  to  $97^\circ$ . A gain, the peaks in absorption correspond to EPR, and the labeling is discussed in ref. [27]. The quality of the data is noticeably poorer than the data in Fig. 29, and is due to the positioning of the sample at a different location in the cavity, where the geometry of the electromagnetic fields are not quite optimal for EPR. Fig. 33 displays (a) a gray scale contour map and (b) a 3D plot representing the same data shown in Fig. 32 (the darker colored regions correspond to stronger EPR absorption), albeit for a wider range of angles (up to  $\theta = 105^\circ$ ). As discussed at great length in ref. [27], the transverse-field EPR spectra for  $Mn_{12}$ -ac exhibit unusual selection rules for frequencies below 90 GHz: two series of resonances are separately observed (labeled  $\alpha$  and  $\beta$ ) as the magnetic field is tilted away from the hard plane. These selection rules are extremely sensitive to the field orientation for angles close to the hard plane. Thus, deviations from the behavior predicted by the giant spin model (Eq. (1)) provide evidence for tilts of the molecules.

51.3 GHz simulations of the EPR spectra for an idealized  $Mn_{12}$ -ac sample are displayed in Fig. 34 both a color contour map for the full  $\theta = 90$  to  $105^\circ$  range (Fig. 34a) and a 3D view for the  $\theta = 90$  to  $97^\circ$  range (Fig. 34b). These 15 K simulations were generated using accepted Hamiltonian parameters given above. A Gaussian line shape was employed with a line width typical for a single solvent-disorder variant in Comia's model (see ref. [27]). While this line shape/width is clearly quite different from the experimental data, which is complicated by the contributions of several  $Mn_{12}$ -ac variants, we note that the choice of line width/shape does not in any way affect the following analysis. The simulations indicate a range of about 1:6 (from  $91.8^\circ$  to  $93.4^\circ$ ) over which the matrix elements for both the  $\alpha$  and  $\beta$  transitions are negligible. Thus, for a perfect crystal, without any disorder, one should expect a similar behavior in the actual EPR spectra. However, careful inspection of Fig. 32 and 33 indicates a significant overlap of the  $\alpha$  and  $\beta$  peaks

in the  $92^\circ$  to  $93^\circ$  range. These two facts point to a spread in the orientations of the magnetic axes of the molecules, with a cut-off of at least 1:3 away from the global directions, i.e. we predict that, on average, the magnetic easy axes of the low-symmetry (disordered) molecules are tilted away from the crystallographic z-axis, and that the distribution of tilts has a half-width-at-half-maximum of  $1:3^\circ$ . Once again, a very similar behavior has been observed for h- $Mn_{12}$ -ac in ref. [27], albeit the distribution is slightly larger (1:7). We note that the h- $Mn_{12}$ -ac experiments were conducted using a rotating cavity [49] to higher magnetic fields, where the experimental deviation from the simulation is even more pronounced. Thus, easy axis tilting appears to be a general feature in  $Mn_{12}$ -ac and, as discussed earlier in this article, this likely provides an explanation for the lack of selection rules in the magnetization steps observed from hysteresis experiments.

Finally, we comment on a possible correlation between the disorder-induced rhombic anisotropy and the easy axis tilting. It was pointed out originally by Comia et al. [16], that one should expect some easy axis tilting to accompany any rhombic distortion. Subsequently, we have shown this to be the case from EPR studies of h- $Mn_{12}$ -ac [27], where it was shown that the high-field fine structure in the transverse EPR spectra display a different angle dependence compared to the main portion of the peaks. This is again apparent for d- $Mn_{12}$ -ac from Fig. 33a, where the shoulders are visible as narrow horizontal streaks on the high field sides of each of the main peaks. It is quite evident that the narrow streaks (i.e. the shoulders) span a narrower angle range compared to the main peaks. In fact, the high field shoulders on the  $\alpha$  and  $\beta$  peaks exhibit a considerable range almost precisely equivalent to 1:6 where neither is observed.

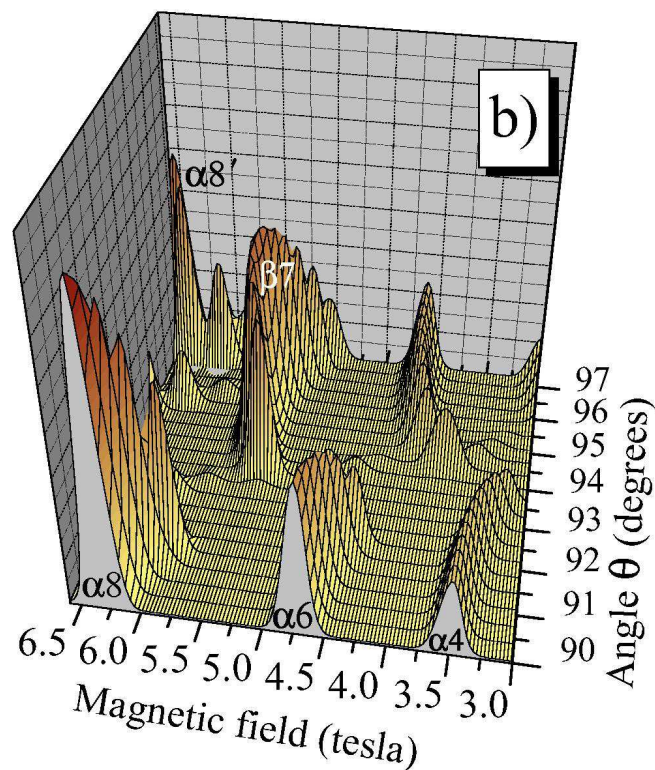
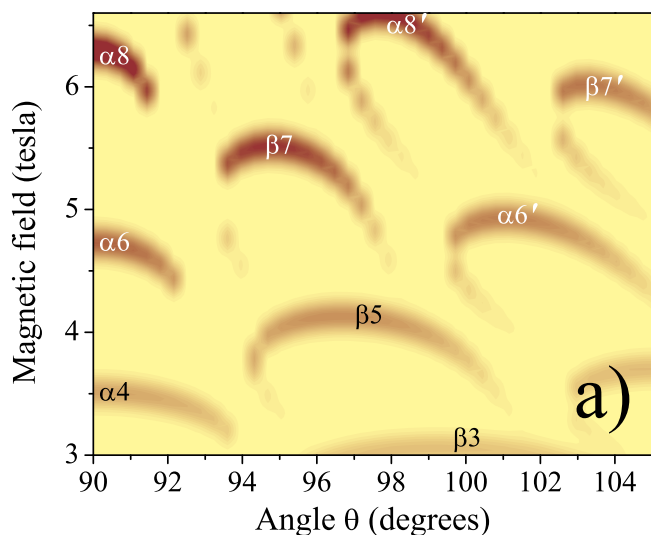


FIG. 34: (Color on-line) (a) A color contour map and (b) a 3D color surface plot representing simulations of the data in Fig. 33, assuming that all molecules are aligned, i.e. no tilting. The simulations were generated using the Hamiltionian parameters given in the text, and the temperature and frequency are 15 K and 51.3 GHz respectively.

Furthermore, comparison between Fig. 32 and 33 indicates that the angle dependence of the high-field shoulders agrees very well with the simulations. The reason for these differences between the main peaks and the shoulders is explained in ref. [27] as being due to discrete easy axis tilting, wherein the tilting is confined to two orthogonal planes defined by the hard and

medium directions of the associated disorder-induced  $\hat{O}_2^2(E)$  zero-field tensor. Essentially, the shoulders on the EPR peaks are due to molecules which are tilted in a plane which is approximately perpendicular to the plane of rotation of the applied magnetic field. Consequently, the tilts due to these molecules do not project onto the field rotation plane, i.e. the experiment is insensitive to tilts in this direction. Meanwhile, the main portion of the EPR peaks is due to molecules which tilt in the orthogonal plane. For these molecules, the tilts have a maximum projection on to the field rotation plane, i.e. the experiment is maximally sensitive to tilts in this direction. The present studies support the findings of the original study for h-Mn<sub>12</sub>-ac, providing further confirmation for the discrete tilting idea.

## V. GENERAL CONCLUSIONS

### A. Discussion on d- and h-Mn<sub>12</sub>-ac differences

This work concludes that all the spin Hamiltonian parameters for h-Mn<sub>12</sub>-ac and d-Mn<sub>12</sub>-ac are essentially identical and in agreement with our previous EPR studies [27], except for the E parameter: E is 0.02 cm<sup>-1</sup> (29 mK) for d-Mn<sub>12</sub>-ac but 0.01 cm<sup>-1</sup> (14 mK) for h-Mn<sub>12</sub>-ac. It is noteworthy also that the average angle of the easy-axis tilts is somewhat larger for h-Mn<sub>12</sub>-ac (1.7 degrees) than for d-Mn<sub>12</sub>-ac (1.3 degrees). We tentatively assign this large (factor of two) increase in the E value on deuteration to the different lengths of a Mn(III)-O (carboxylate) bond in h-Mn<sub>12</sub>-ac and d-Mn<sub>12</sub>-ac. Crystals of d-Mn<sub>12</sub>-ac are prepared from a 60% CD<sub>3</sub>COOD/D<sub>2</sub>O solution. Acidic deuterium rapidly exchanges with ambient humidity. Single crystal neutron diffraction studies [50] have shown that both the CD<sub>3</sub>COOD and D<sub>2</sub>O molecules in the crystal have changed to CD<sub>3</sub>COOH and H<sub>2</sub>O. Thus, for the crystals studied in the neutron structure determination the formula is [Mn<sub>12</sub>O<sub>12</sub>(O<sub>2</sub>CCD<sub>3</sub>)<sub>16</sub>(H<sub>2</sub>O)<sub>4</sub> · 2CD<sub>3</sub>COOH · 4H<sub>2</sub>O. In the other experiments starting with perdeuterated crystals the amount of exchange was not determined. We note that partial deuterium exchange is an additional source of disorder in deuterated crystals that could affect the magnetic anisotropy, again by lowering the local symmetry.

There are three different types of Mn atoms in the asymmetric unit in the tetragonal Mn<sub>12</sub>-ac molecule (see inset of Figs. 35, 36, and 37). The first type, labeled Mn1, is a Mn(IV) atoms residing in the central cubane core. The other two types, both Mn(III), are situated in a ring that surrounds the cubane unit. Each of these Mn(III) has an elongated Jahn-Teller axis. One of these Mn(III) atoms, labeled Mn3, has a water molecule coordinated to it. The acetic acid solvate molecule is hydrogen bonded to the oxygen atom (labeled O\* in Fig. 37) which makes up the carboxylate which is

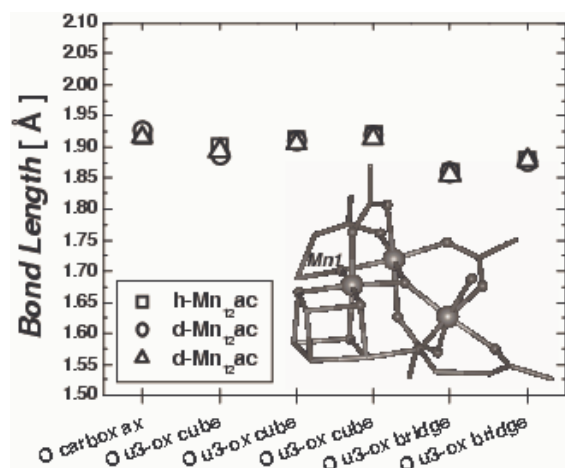


FIG. 35: Reproductions of the bond lengths in the coordination sphere of Mn1 from references [50, 51, 52]. The symbols squares (83 K, x-ray diffraction), circles (20 K, neutron diffraction), and triangles (249 K, x-ray diffraction) represent data from ref [51], [50] and [52] respectively.

bound to the other type of Mn(III) ion, labeled Mn2. Three crystal structures [50, 51, 52] were analyzed to see if there were any structural differences between the h-Mn<sub>12</sub>-ac and d-Mn<sub>12</sub>-ac. These data collections for the three crystal structures were carried out at three different temperatures. The data for the x-ray structure in ref. [51] were collected at 83 K while the ref. [52] data were collected at 249 K. The neutron diffraction study from ref. [50] was carried out at 20 K. The Mn-O bond metrics compared between the h-Mn<sub>12</sub>-ac and d-Mn<sub>12</sub>-ac structures are in agreement with one exception. In Fig. 35, the bond distances of Mn1-O are shown for the three crystal structures. There is very little difference between the d-Mn<sub>12</sub>-ac and h-Mn<sub>12</sub>-ac crystal structures for the Mn1 atom. The Mn1 atom resides in a tight cubane core where it would be difficult to change dimensions. The bond lengths of Mn3-O, represented in Fig. 36, are also in agreement between the d-Mn<sub>12</sub>-ac and h-Mn<sub>12</sub>-ac structures. As can be seen in Fig. 37, the bond distances for Mn2, however, are different between the d-Mn<sub>12</sub>-ac and h-Mn<sub>12</sub>-ac structures. An Mn(III)-O (carboxylate) bond, labeled Mn2 and O\* in Fig. 37, which is part of its Jahn-Teller elongation axis to which the acetic acid solvate molecule (CD<sub>3</sub>COOH for d-Mn<sub>12</sub>-ac and CH<sub>3</sub>COOH for h-Mn<sub>12</sub>-ac) is hydrogen bonded is significantly longer for the d-Mn<sub>12</sub>-ac (2.19 Å for d-Mn<sub>12</sub>-ac versus 2.14 Å for the h-Mn<sub>12</sub>-ac). It is possible that this bond difference will have an effect on the zero field splitting parameters of the d-Mn<sub>12</sub>-ac relative to the h-Mn<sub>12</sub>-ac molecule. The Mn2-O\* bond length is different for d-Mn<sub>12</sub>-ac. The single-ion zero field splitting of this Mn2 ion is therefore different and its vectorial projection onto the molecule as a whole should yield molecular ZFS parameters that differ between h-Mn<sub>12</sub>-ac and d-Mn<sub>12</sub>-ac.

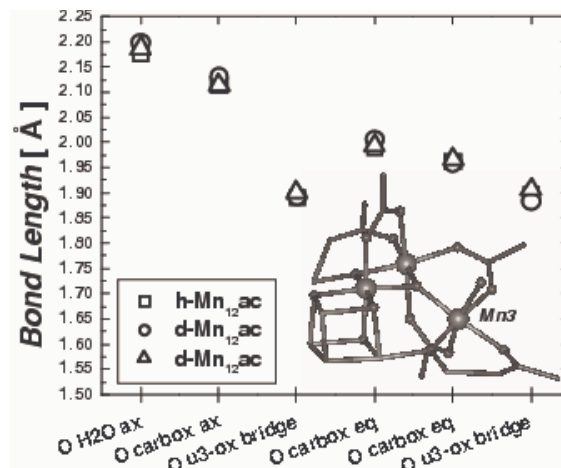


FIG. 36: Reproductions of the bond lengths in the coordination sphere of Mn3 from references [50, 51, 52]. The symbols squares (83 K, x-ray diffraction), circles (20 K, neutron diffraction), and triangles (249 K, x-ray diffraction) represent data from ref [51], [50] and [52] respectively.

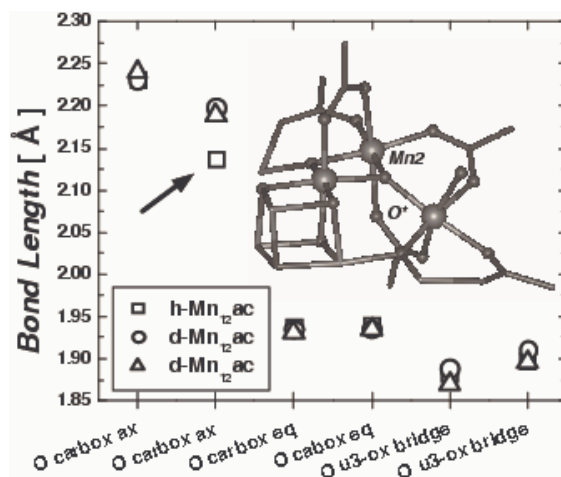


FIG. 37: Reproductions of the bond lengths in the coordination sphere of Mn2 from references [50, 51, 52]. The symbols squares (83 K, x-ray diffraction), circles (20 K, neutron diffraction), and triangles (249 K, x-ray diffraction) represent data from ref [51], [50] and [52] respectively. The arrow emphasizes an important difference between the h-Mn<sub>12</sub>-ac and d-Mn<sub>12</sub>-ac structures. See the text for details.

## B. Summary of results

In summary, these experiments provide a comprehensive understanding of the factors that influence the symmetry of MQT in Mn<sub>12</sub>-acetate, the first and most widely studied SMM. Interestingly, the reason so much attention has focused on Mn<sub>12</sub> has been the high global symmetry of single crystals, as most known SMMs have lower site symmetry. The data presented here show that disorder lowers the symmetry locally and leads to an intricate interaction between transverse anisotropy terms: the first associated with disorder and the second intrinsic to an "ideal" Mn<sub>12</sub>-molecule. While at first

sight a nuisance, these complexities have been interesting from many perspectives. From experiment, they have been a challenge to understand and characterize and have required combining unique advanced and sensitive magnetic techniques that have been developed by the authors over many years. In particular, this research involved combining single crystal high frequency and high field EPR and low-temperature magnetometry, both with arbitrarily directed applied magnetic fields. The results obtained by magnetic measurements of MQT have had implications for EPR studies and vice-versa. From a theoretical perspective, given a structural model of the molecule and solvent environment, density functional theory has been able to capture many of the features observed in these experiments, including

the magnitudes and form of the transverse magnetic anisotropies and the easy axis tilts [45]. This includes the angle between the 2nd order and 4th order transverse anisotropies, which has been central to understanding the combined data set, as well as the easy axis tilts. This research thus represents an important milestone in our understanding of the factors that influence MQT in SMMs.

**Acknowledgments.** This research was supported by NSF (Grant Nos. DMR-0103290, 0114142, 0239481 and 0315609). S.H. acknowledges Research Corporation for financial support.

- 
- [1] J. Tejada, E. M. Chudnovsky, E. del Barco, and J. M. Hernandez, *Nanotechnology* 12, 181 (2001)
- [2] D. Loss, M. Leuenberger, and D. DiVincenzo, *Nature* 410, 789 (2000)
- [3] J. R. Friedman, M. P. Sarachik, J. Tejada, and R. Ziolo, *Phys. Rev. Lett.* 76, 3830 (1996).
- [4] J. M. Hernandez et al., *Europhys. Lett.* 35, 301 (1996).
- [5] L. Thomas, F. Lioni, R. Balku, D. Gatteschi, R. Sessoli and B. Barbara, *Nature (London)* 383, 145 (1996).
- [6] C. Sangregorio, T. Ohm, C. Paulsen, R. Sessoli and D. Gatteschi, *Phys. Rev. Lett.* 78, 4645 (1997).
- [7] A. L. Barra, D. Gatteschi, and R. Sessoli, *Phys. Rev. B* 56, 8192 (1997).
- [8] J. A. A. J. Perenboom, J. S. Brooks, S. Hill, T. Hathaway and N. S. Dalal, *Phys. Rev. B* 58, 330 (1998);
- [9] K. M. Mertes et al., *Phys. Rev. Lett.* 87, 227205 (2001).
- [10] J. M. Hernandez, F. Torres, J. Tejada, and E. Molins, *Phys. Rev. B* 66, 161407 (2002).
- [11] L. Bokacheva, A. D. Kent, and M. A. Walters, *Phys. Rev. Lett.* 85, 4803 (2000); A. D. Kent et al., *Europhys. Lett.* 49, 521 (2000).
- [12] I. Mirabeau et al., *Phys. Rev. Lett.* 83, 628 (1999).
- [13] S. Hill, J. A. A. Perenboom, N. S. Dalal, T. Hathaway, T. Stalcup, and J. S. Brooks, *Phys. Rev. Lett.* 80, 2453 (1998).
- [14] E. M. Chudnovsky, and D. A. Garanin, *Phys. Rev. Lett.* 87, 187203 (2001).
- [15] E. M. Chudnovsky, and D. A. Garanin, *Phys. Rev. B* 65, 094423 (2002).
- [16] A. Comia, R. Sessoli, L. Sorace, D. Gatteschi, A. L. Barra, *Phys. Rev. Lett.* 89, 257201 (2002).
- [17] E. del Barco, A. D. Kent, E. M. Lumberger, D. N. Hendrikson and G. Christou, *Europhys. Lett.* 60, 768 (2002).
- [18] E. del Barco, A. D. Kent, E. M. Lumberger, D. N. Hendrikson and G. Christou, *Phys. Rev. Lett.* 91, 047203 (2003).
- [19] S. Hill, R. S. Edwards, S. I. Jones, N. S. Dalal, and J. M. North, *Phys. Rev. Lett.* 90, 217204 (2003).
- [20] K. Park et al., *Phys. Rev. B* 65, 014426 (2002).
- [21] S. Hill et al., *Phys. Rev. B* 65, 224410 (2002).
- [22] R. Amigo et al., *Phys. Rev. B* 65, 172403 (2001).
- [23] S. M. accagnano, R. A. chey, E. N. egusse, A. Lussier, M. M. Mola, S. Hill, and N. S. Dalal, *Polyhedron* 20, 1441 (2001).
- [24] K. Park, M. A. Novotny, N. S. Dalal, S. Hill, and P. A. Rikvold, *J. Appl. Phys.* 91, 7167 (2002).
- [25] B. Parks, J. Loomis, E. Rumberger, D. N. Hendrickson and G. Christou, *Phys. Rev. B* 64, 184426 (2001).
- [26] A. A. Mukhin et al., *Europhys. Lett.* 44, 778 (1998).
- [27] S. Hill, S. Takahashi, R. S. Edwards, J. M. North and N. S. Dalal, *arXiv:cond-mat/0401515* (2004).
- [28] E. del Barco, A. D. Kent, N. Chakov, G. Christou, and D. N. Hendrikson, *Phys. Rev. B* 69, 020411 (R) (2004).
- [29] T. Lis, *Acta Crystallogr., Sect. B: Struct. Crystallogr. Cryst. Chem.* 36, 2042 (1980).
- [30] G. Christou, et al., *MRS Bull.* 25, 66 (2000).
- [31] N. Regnault, Th. Julicoeur, R. Sessoli, D. Gatteschi and M. Verdager, *Phys. Rev. B* 66, 054409 (2002).
- [32] J. Liu, B. Wu, L. Fu, R. B. Diener, and Q. Ni, *Phys. Rev. B* 65, 224401 (2002).
- [33] W. Wemdsorfer and R. Sessoli, *Science* 284, 133 (1999).
- [34] S. Hill, private communication.
- [35] D. Garanin and E. M. Chudnovsky, *Phys. Rev. B* 57, 11102 (1997).
- [36] D. Loss, D. P. DiVincenzo and G. G. Rinstein, *Phys. Rev. Lett.* 69, 3232 (1992).
- [37] A. Garg, *Europhys. Lett.* 22, 205 (1993).
- [38] W. Wemdsorfer, M. Soler, G. Christou, D. N. Hendrikson, *J. Appl. Phys.* 29, 7164 (2002).
- [39] C. S. Park and A. Garg, *Phys. Rev. B* 65, 064411 (2002).
- [40] A. D. Kent, S. von Molnar, S. Gider and D. D. Awschalom, *Jour. Appl. Phys.* 76, 6656 (1994).
- [41] d-M<sub>n12</sub>-acetate was synthesized by following the standard procedure for preparing h-M<sub>n12</sub>-acetate, but using D<sub>2</sub>O and deuterated acetic, CD<sub>3</sub>COOD, as outlined in [27].
- [42] C. Zener, *Proc. R. Soc. London A* 137, 696 (1932); S. Miyashita, *J. Phys. Soc. Jpn.* 64, 3207 (1995); V. V. Dobrovitski and A. K. Zvezdin, *Europhys. Lett.* 38, 377 (1997); L. Gunther *ibid.* 39, 1 (1997); G. Rose and P. C. E. Stamp, *J. Low Temp. Phys.* 113, 1153 (1998).
- [43] In the result presented in ref. [18] the onefold contribution of this measurement was displaced by 180 degrees. This corresponds to a mistake that was due to the fact that for this experiment we took  $\theta = 180$  (that corresponds to negative orientation of one of the coils of the

superconducting vector magnet) as the origin of rotation while for all the others the origin was  $\theta = 0$  (positive orientation of the same coil) and we did not correct it in the data.

- [44] We studied the behavior of the MQT probability with a transverse field applied along the directions of a maximum and a minimum of the twofold MQT probability response because our initial interpretation of the results in ref. [18] neglected the effect of two non-collinear anisotropies and we assumed that those were the directions of the hard and the medium anisotropy axes associated with  $E(S_x^2 - S_y^2)$ . As we explain in this article, these directions, in fact, correspond to medium anisotropy axes of the fourth anisotropy term and none of them are along the hard anisotropy axes of the second anisotropy term.
- [45] K. Park, T. Baruah, N. Bernstein and M.R. Pederson, arXiv:cond-mat/0312261 (2004).
- [46] M. Mola, S. Hill, P. Goy and M. Gross, Rev. Sci. Instr. 71, 186 (2000).
- [47] R.S. Edwards et al. (unpublished)
- [48] S. Hill et al., (in preparation)
- [49] S. Takahashi et al., (in preparation)
- [50] P. Langan, R. Robinson, P. J. Brown, D. Argyriou, D. Hendrickson, G. Christou, Acta Crystallogr. Sect. C - Cryst. Struct. Comm. 57, 909 (2001).
- [51] A. Comia et al., Acta Crystallogr. Sect. C - Cryst. Struct. Comm. 58, m 371 (2002).
- [52] D. Hendrickson and A.L. Rheingold, (unpublished)